

Gravitational waves from first-order phase transition in an electroweakly interacting vector dark matter model

Tomohiro Abe^a Katsuya Hashino^{a,b}

^a*Department of Physics, Faculty of Science and Technology, Tokyo University of Science, Noda, Chiba 278-8510, Japan*

^b*National Institute of Technology, Fukushima College, Nagao 30, Taira-Kamiarakawa, Iwaki, Fukushima 970-8034, Japan*

E-mail: abe.tomohiro@rs.tus.ac.jp, hashino@fukushima-nct.ac.jp

ABSTRACT: We consider gravitational waves in an electroweakly interacting vector dark matter (DM) model. The gauge symmetry of the model is $SU(3)_C \times SU(2)_0 \times SU(2)_1 \times SU(2)_2 \times U(1)_Y$, and an exchange symmetry between $SU(2)_0$ and $SU(2)_2$ is imposed to ensure the stability of the DM. Above the electroweak scale, phase transition $SU(2)_0 \times SU(2)_1 \times SU(2)_2 \rightarrow SU(2)_L$ occurs. All new particles in the model are bosons, and the new gauge couplings can be relatively large within the perturbative regime. Thus, a potential barrier is easily produced during the phase transition. Consequently, the phase transition can be strongly first-order and produces detectable gravitational waves. The results depend on $m_{h'}$, which is the mass of the Z_2 -even new scalar particle under the exchange symmetry, and on m_V , which is the mass of the vector DM. We find that the model can be tested by future observations of the gravitational waves from the first-order phase transition if $2.5 \text{ TeV} \lesssim m_{h'} \lesssim 3.5 \text{ TeV}$ for $m_V = 7 \text{ TeV}$, $1.6 \text{ TeV} \lesssim m_{h'} \lesssim 2.5 \text{ TeV}$ for $m_V = 5 \text{ TeV}$, and $2.8 \text{ TeV} \lesssim m_{h'} \lesssim 3.5 \text{ TeV}$ for $m_V = 3 \text{ TeV}$, respectively.

Contents

1	Introduction	1
2	The model	3
2.1	Scalar boson masses	4
2.2	Gauge boson masses	5
2.3	Parameters	6
3	Loop and finite temperature corrections to scalar potential and phase transition	8
3.1	Effective potential	8
3.2	First-order phase transition	11
4	Gravitational wave spectrum	13
5	Results	17
6	Conclusion	21
A	Approximated expressions of the gauge bosons for $v_\Phi \gg v$	22
B	$V_{\text{CW}} + \delta V$	23

1 Introduction

Many astrophysical observations show the existence of dark matter (DM). DM constitutes approximately 26% of the energy in the universe [1]. However, the nature of DM remains unclear. Models beyond the standard model (SM) of particle physics often predict new particles that are DM candidates. In many particle DM models, the freeze-out mechanism [2] is used to explain the measured value of the DM energy density. The mechanism requires a pair of DM particles to annihilate into other particles in the thermal bath in the early Universe. The canonical value of the annihilation cross section, which can explain the measured value of the DM energy density, is $\langle\sigma v\rangle \simeq 3 \times 10^{-26} \text{ cm}^3 \text{ s}^{-1} \simeq 1 \text{ pb } c$. This value is of the same order as the cross section of the electroweak interaction, which implies that DM particles interact with the SM particles via the electroweak interaction. An example of such DM is the wino DM, which is an $\text{SU}(2)_L$ triplet spin- $\frac{1}{2}$ Majorana fermion, and the mass prediction of the thermally produced wino DM is approximately 3 TeV [3, 4].

An electroweakly interacting spin-1 vector DM model was proposed in [5]. In this model, the electroweak symmetry is extended to $\text{SU}(2)_0 \times \text{SU}(2)_1 \times \text{SU}(2)_2 \times \text{U}(1)_Y$. This extended electroweak symmetry is spontaneously broken by scalar fields Φ_1 and Φ_2 into

the electroweak symmetry, $SU(2)_0 \times SU(2)_1 \times SU(2)_2 \times U(1)_Y \rightarrow SU(2)_L \times U(1)_Y$. The Lagrangian is invariant under the exchange between $SU(2)_0$ and $SU(2)_2$. This exchange symmetry is the Z_2 symmetry, which stabilizes the DM. A linear combination of $SU(2)_0$ and $SU(2)_2$ gauge bosons denoted as V_μ^a is Z_2 -odd under the exchange symmetry. It is an approximately $SU(2)_L$ triplet, and thus is similar to the wino DM but has spin-1. The electrically neutral component of V_μ^a is slightly lighter than its charged component owing to radiative corrections at the loop level; thus, it is a DM candidate. The mass of the spin-1 DM was predicted to be between 3 and 19 TeV to obtain the right amount of DM energy density via the freeze-out mechanism [5]. The allowed mass range is broader than one in the wino DM model because DM particles can annihilate into extra gauge bosons, W' and Z' . The constraints of new particle searches in collider experiments and indirect searches of the DM were studied in [5, 6]. However, a wide range of parameter spaces remains unexplored.

In this paper, we focus on the phase transition of scalar potential. In particular, we investigate gravitational wave (GW) generated during the first-order phase transition of $SU(2)_0 \times SU(2)_1 \times SU(2)_2 \rightarrow SU(2)_L$. In general, the approximate effective potential at high temperature is described as

$$V_{\text{eff}}(\varphi, T) \simeq D(T^2 - T_0^2)\varphi^2 - ET\varphi^3 + \lambda_T\varphi^4, \quad (1.1)$$

where φ is the order parameter for the phase transition and T is the temperature. D , T_0 , E , and λ_T are model dependent parameters. The cubic term $ET\varphi^3$ is necessary to realize the first-order phase transition and is generated by the thermal loop effects of bosons even if the cubic term is absent at zero temperature. In the electroweakly interacting vector DM model, all new particles are bosons, and the new gauge couplings can be relatively large, although they remain within the perturbative regime [5]. Thus, the cubic term is expected to be sufficiently large to realize a first-order phase transition.

First-order phase transitions generate gravitational waves (GWs) [7]. Future space-based GW interferometers, such as LISA [8], DECIGO [9], and BBO [10], can be used to observe GW spectra; thus, a DM model with a first-order phase transition can be tested through GW observational experiments [11–65].

We found that GWs can be generated in the electroweakly interacting vector DM model with large gauge couplings of $SU(2)_0$ and $SU(2)_1$ symmetries. If the mass of h' , which is the Z_2 -even under exchange symmetry, is a few TeV, the model can predict the detectable GWs in future experiments. Some regions of the parameter space can be tested by both GWs and W' searches in the collider experiments.

The rest of this paper is organized as follows. In Section 2, we briefly introduce the vector DM model with $SU(2)_0 \times SU(2)_1 \times SU(2)_2 \times U(1)_Y$ gauge symmetry. In Section 3, we show the effective potential with finite-temperature effects for this model. We clarify the parameter region with a first-order phase transition, which can produce a detectable GW spectrum. The formula for the GW spectrum from the first-order phase transition is presented in Section 4. We discuss in Section 5 the testability of the model at the GW observation experiments, such as the LISA, DECIGO, and BBO experiments. Finally, Section 6 presents the conclusions of this study.

field	spin	SU(3) _c	SU(2) ₀	SU(2) ₁	SU(2) ₂	U(1) _Y
q_L	$\frac{1}{2}$	3	1	2	1	$\frac{1}{6}$
u_R	$\frac{1}{2}$	3	1	1	1	$\frac{2}{3}$
d_R	$\frac{1}{2}$	3	1	1	1	$-\frac{1}{3}$
ℓ_L	$\frac{1}{2}$	1	1	2	1	$-\frac{1}{2}$
e_R	$\frac{1}{2}$	1	1	1	1	-1
H	0	1	1	2	1	$\frac{1}{2}$
Φ_1	0	1	2	2	1	0
Φ_2	0	1	1	2	2	0

Table 1. Charge assignment under the SU(3)_c × SU(2)₀ × SU(2)₁ × SU(2)₂ × U(1)_Y gauge symmetry of the model.

2 The model

In this section, we briefly introduce the electroweakly interacting vector DM model proposed in [5].

The model exhibits gauge symmetry, described as SU(3)_c × SU(2)₀ × SU(2)₁ × SU(2)₂ × U(1)_Y. Here, SU(3)_c and U(1)_Y correspond to the gauge symmetries governing the quantum chromodynamics (QCD) and hypercharge, respectively. Because the QCD sector is the same as that in the SM, we focus on the electroweak sector, denoted as SU(2)₀ × SU(2)₁ × SU(2)₂ × U(1)_Y. For this electroweak sector, we use the notation $W_{j\mu}^a$ for gauge bosons associated with SU(2)_j and B_μ for those linked to U(1)_Y. Here, j can take values of 0, 1, or 2, and a can take values of 1, 2, or 3. g_j and g' are the gauge couplings for SU(2)_j and U(1)_Y, respectively.

We introduce two scalar fields, Φ_1 and Φ_2 , expressed in two-by-two matrices. They transform under gauge transformation as

$$\Phi_1 \rightarrow U_0 \Phi_1 U_1^\dagger, \quad \Phi_2 \rightarrow U_2 \Phi_1 U_1^\dagger, \quad (2.1)$$

where U_0, U_1 , and U_2 represent two-by-two unitary matrices for SU(2)₀, SU(2)₁, and SU(2)₂, respectively. In addition, we impose the following conditions for Φ_j to reduce their degrees of freedom,

$$\Phi_j = -\epsilon \Phi_j^* \epsilon, \quad \text{where } \epsilon = \begin{pmatrix} 0 & 1 \\ -1 & 0 \end{pmatrix}. \quad (2.2)$$

Hence, each Φ_j consists of four real scalar fields.

All other fields remain identical to those in the SM, except that they are charged under SU(2)₁ instead of SU(2)_L. The charge assignments for the matter fields are summarized in Table 1.

In addition to gauge symmetry, this model exhibits exchange symmetry. The Lagrangian is invariant under the following field transformations:

$$W_{0\mu}^a \rightarrow W_{2\mu}^a, \quad W_{2\mu}^a \rightarrow W_{0\mu}^a, \quad \Phi_1 \rightarrow \Phi_2, \quad \Phi_2 \rightarrow \Phi_1, \quad (2.3)$$

whereas all other fields remain unchanged. This symmetry is equivalent to the exchange between $SU(2)_0$ and $SU(2)_2$, implying that the gauge couplings of $SU(2)_0$ and $SU(2)_2$ must be identical. It is important to note that under this symmetry, $\frac{W_{0\mu}^a - W_{2\mu}^a}{\sqrt{2}}$ and $\frac{\Phi_1 - \Phi_2}{\sqrt{2}}$ change sign, whereas $\frac{W_{0\mu}^a + W_{2\mu}^a}{\sqrt{2}}$, $\frac{\Phi_1 + \Phi_2}{\sqrt{2}}$, and the other fields remain unchanged. Therefore, the symmetry described in Eq. (2.3) is equivalent to the Z_2 symmetry commonly used in DM models. The lightest particle among $\frac{W_{0\mu}^a - W_{2\mu}^a}{\sqrt{2}}$ and $\frac{\Phi_1 - \Phi_2}{\sqrt{2}}$ is stable and is a dark matter candidate for this model.

The Lagrangian of the scalar and the electroweak gauge sectors are described as

$$-\frac{1}{4} \sum_{j=0}^2 W_{j\mu\nu}^a W_j^{a\mu\nu} - \frac{1}{4} B_{\mu\nu} B^{\mu\nu} + \sum_{j=1}^2 \frac{1}{2} \text{tr} \left(D^\mu \Phi_j^\dagger D_\mu \Phi_j \right) - V_{\text{scalar}}, \quad (2.4)$$

where

$$\begin{aligned} V_{\text{scalar}} = & m^2 H^\dagger H + m_\Phi^2 \text{tr} \left(\Phi_1^\dagger \Phi_1 \right) + m_\Phi^2 \text{tr} \left(\Phi_2^\dagger \Phi_2 \right) + \lambda (H^\dagger H)^2 \\ & + \lambda_\Phi \left(\text{tr} \left(\Phi_1^\dagger \Phi_1 \right) \right)^2 + \lambda_\Phi \left(\text{tr} \left(\Phi_2^\dagger \Phi_2 \right) \right)^2 + \lambda_{h\Phi} H^\dagger H \text{tr} \left(\Phi_1^\dagger \Phi_1 \right) \\ & + \lambda_{h\Phi} H^\dagger H \text{tr} \left(\Phi_2^\dagger \Phi_2 \right) + \lambda_{12} \text{tr} \left(\Phi_1^\dagger \Phi_1 \right) \text{tr} \left(\Phi_2^\dagger \Phi_2 \right). \end{aligned} \quad (2.5)$$

Some couplings are equal owing to the exchange symmetry described in Eq. (2.3).

We assume that the scalar fields develop the following vacuum expectation values (VEVs),

$$\langle H \rangle = \begin{pmatrix} 0 \\ \frac{v}{\sqrt{2}} \end{pmatrix}, \quad \langle \Phi_1 \rangle = \langle \Phi_2 \rangle = \frac{1}{\sqrt{2}} \begin{pmatrix} v_\Phi & 0 \\ 0 & v_\Phi \end{pmatrix}. \quad (2.6)$$

These VEVs do not break the exchange symmetry and maintain the Z_2 symmetry, which stabilizes the DM candidate. We parametrized the component fields of each scalar field as

$$H = \begin{pmatrix} i\pi_3^+ \\ \frac{v + \sigma_3 - i\pi_3^0}{\sqrt{2}} \end{pmatrix}, \quad \Phi_j = \begin{pmatrix} \frac{v_\Phi + \sigma_j + i\pi_j^0}{\sqrt{2}} & i\pi_j^+ \\ i\pi_j^- & \frac{v_\Phi + \sigma_j - i\pi_j^0}{\sqrt{2}} \end{pmatrix}. \quad (2.7)$$

where $\pi_3^\pm, \pi_3^0, \pi_j^\pm, \pi_j^0$, and π_j^0 are would-be Nambu-Goldstone (NG) bosons. Based on the stationary condition, we obtain the followings:

$$m^2 = -\lambda v^2 - 2\lambda_{h\Phi} v_\Phi^2, \quad (2.8)$$

$$m_\Phi^2 = -\frac{\lambda_{h\Phi}}{2} v^2 - (\lambda_{12} + 2\lambda_\Phi) v_\Phi^2. \quad (2.9)$$

2.1 Scalar boson masses

The mass terms for scalar fields other than the would-be NG bosons are described as

$$-\frac{1}{2} \begin{pmatrix} \sigma_3 & \sigma_1 & \sigma_2 \end{pmatrix} \mathcal{M}_\sigma^2 \begin{pmatrix} \sigma_3 \\ \sigma_1 \\ \sigma_2 \end{pmatrix}, \quad (2.10)$$

where

$$\mathcal{M}_\sigma^2 = \begin{pmatrix} 2\lambda v^2 & 2vv_\Phi \lambda_{h\Phi} & 2vv_\Phi \lambda_{h\Phi} \\ 2vv_\Phi \lambda_{h\Phi} & 8v_\Phi^2 \lambda_\Phi & 4v_\Phi^2 \lambda_{12} \\ 2vv_\Phi \lambda_{h\Phi} & 4v_\Phi^2 \lambda_{12} & 8v_\Phi^2 \lambda_\Phi \end{pmatrix}. \quad (2.11)$$

Diagonalizing this mass matrix, we obtain the mass eigenstates denoted as h , h' , and h_D . The relation between $(\sigma_3, \sigma_1, \sigma_2)$ and (h, h', h_D) is

$$\begin{pmatrix} \sigma_3 \\ \sigma_1 \\ \sigma_2 \end{pmatrix} = R \begin{pmatrix} h \\ h' \\ h_D \end{pmatrix}, \quad (2.12)$$

where R is determined to diagonalize the mass matrix,

$$R^T \mathcal{M}_\sigma^2 R = \begin{pmatrix} m_h^2 & 0 & 0 \\ 0 & m_{h'}^2 & 0 \\ 0 & 0 & m_{h_D}^2 \end{pmatrix}. \quad (2.13)$$

R is expressed as

$$R = \begin{pmatrix} \cos \phi_h & -\sin \phi_h & 0 \\ \frac{1}{\sqrt{2}} \sin \phi_h & \frac{1}{\sqrt{2}} \cos \phi_h & \frac{1}{\sqrt{2}} \\ \frac{1}{\sqrt{2}} \sin \phi_h & \frac{1}{\sqrt{2}} \cos \phi_h & -\frac{1}{\sqrt{2}} \end{pmatrix}. \quad (2.14)$$

The couplings in the potential are expressed in terms of the masses of the physical scalars and ϕ_h using Eqs. (2.11) and (2.12),

$$\lambda = \frac{m_h^2 \cos^2 \phi_h + m_{h'}^2 \sin^2 \phi_h}{2v^2}, \quad (2.15)$$

$$\lambda_{h\Phi} = -\frac{\sin \phi_h \cos \phi_h}{2\sqrt{2}vv_\Phi} (m_{h'}^2 - m_h^2), \quad (2.16)$$

$$\lambda_\Phi = \frac{m_h^2 \sin^2 \phi_h + m_{h'}^2 \cos^2 \phi_h + m_{h_D}^2}{16v_\Phi^2}, \quad (2.17)$$

$$\lambda_{12} = \frac{m_h^2 \sin^2 \phi_h + m_{h'}^2 \cos^2 \phi_h - m_{h_D}^2}{8v_\Phi^2}. \quad (2.18)$$

2.2 Gauge boson masses

The mass terms of the gauge bosons are given by

$$\mathcal{L} \supset (W_{0\mu}^+ \ W_{1\mu}^+ \ W_{2\mu}^+) \mathcal{M}_C^2 \begin{pmatrix} W_0^{-\mu} \\ W_1^{-\mu} \\ W_2^{-\mu} \end{pmatrix} + \frac{1}{2} (W_{0\mu}^3 \ W_{1\mu}^3 \ W_{2\mu}^3 \ B_\mu) \mathcal{M}_N^2 \begin{pmatrix} W_0^{3\mu} \\ W_1^{3\mu} \\ W_2^{3\mu} \\ B^\mu \end{pmatrix}, \quad (2.19)$$

where

$$\mathcal{M}_C^2 = \frac{1}{4} \begin{pmatrix} g_0^2 v_\Phi^2 & -g_0 g_1 v_\Phi^2 & 0 \\ -g_0 g_1 v_\Phi^2 & 2g_1^2 v_\Phi^2 & -g_1 g_0 v_\Phi^2 \\ 0 & -g_1 g_0 v_\Phi^2 & g_0^2 v_\Phi^2 \end{pmatrix}, \quad (2.20)$$

$$\mathcal{M}_N^2 = \frac{1}{4} \begin{pmatrix} g_0^2 v_\Phi^2 & -g_0 g_1 v_\Phi^2 & 0 & 0 \\ -g_0 g_1 v_\Phi^2 & 2g_1^2 v_\Phi^2 & -g_1 g_0 v_\Phi^2 & -g_1 g' v^2 \\ 0 & -g_1 g_0 v_\Phi^2 & g_0^2 v_\Phi^2 & 0 \\ 0 & -g_1 g' v^2 & 0 & g'^2 v^2 \end{pmatrix}. \quad (2.21)$$

Note that $g_0 = g_2$ based on the exchange symmetry described in Eq. (2.3). After diagonalizing these mass matrices, we obtain ten mass eigenstates: γ , Z , Z' , W^\pm , W'^\pm , V^0 , and V^\pm , where γ is photon, Z and W^\pm are the electroweak gauge bosons in the SM. The Z_2 -odd combinations are described as

$$V_\mu^0 = \frac{W_{0\mu}^3 - W_{2\mu}^3}{\sqrt{2}}, \quad (2.22)$$

$$V_\mu^\pm = \frac{W_{0\mu}^\pm - W_{2\mu}^\pm}{\sqrt{2}}, \quad (2.23)$$

where $W_{j\mu}^\pm = \frac{W_{j\mu}^1 \mp iW_{j\mu}^2}{\sqrt{2}}$. The masses of V^0 and V^\pm at the tree level are expressed as

$$m_{V^0}^2 = m_{V^\pm}^2 = \frac{g_0^2 v_\Phi^2}{4}. \quad (2.24)$$

At the loop level, the electroweak interaction gives different corrections to the masses, and V^\pm is slightly heavier than V^0 [5],

$$m_{V^\pm} - m_{V^0} \simeq 166 \text{ MeV}. \quad (2.25)$$

This mass splitting allows V^\pm to decay into V^0 by emitting a charged pion, and thus V^\pm cannot be regarded as DM.

2.3 Parameters

There are nine parameters in the electroweak sector,

$$(g_0, g_1, g', m^2, m_\Phi^2, \lambda, \lambda_\Phi, \lambda_{h\Phi}, \lambda_{12}). \quad (2.26)$$

Instead of using these nine parameters as inputs, we adopt the following set:

$$(e, v, m_Z, m_V, m_{Z'}, m_h, m_{h'}, m_{h_D}, \phi_h), \quad (2.27)$$

where e is the QED coupling described as $e = \left(\frac{2}{g_0^2} + \frac{1}{g_1^2} + \frac{1}{g_2^2}\right)^{-\frac{1}{2}}$, m_Z is the mass of the Z boson, m_h is the Higgs boson mass, and v is derived from the Fermi constant G_F as $v = (\sqrt{2}G_F)^{-1/2}$. These four parameters were experimentally measured. The remaining five parameters are treated as the model parameters.

The lightest Z_2 -odd particle is the DM candidate for this model. Because $m_{V^\pm} > m_{V^0}$ by the loop effect, the lighter one of V^0 and h_D is the DM candidate in this model. Based on [5], we assume that $m_{V^0} < m_{h_D}$ and treat V^0 as a DM candidate.

As discussed in [5], this model can explain the measured value of the DM energy density through the freeze-out mechanism for $3 \text{ TeV} \lesssim m_{Z'} \lesssim 19 \text{ TeV}$, which is larger than m_W and m_Z . This heavy Z' is realized by the large hierarchy between the two VEVs. Therefore, we investigate the model with $v_\Phi \gg v$.

There are several constraints on ϕ_h . One of the constraints comes from the Higgs coupling. In this model, the h couplings to the SM particles are proportional to $\cos \phi_h$, and they are equal to that in the SM when $\phi_h = 0$. For example, the h coupling to W boson, g_{WWh} , is described as

$$g_{WWh} = \frac{2m_W^2}{v} \cos \phi_h = g_{WWh}^{\text{SM}} \cos \phi_h. \quad (2.28)$$

Other couplings of h are obtained by multiplying the SM predicted values by $\cos \phi_h$. Collider experiments can measure those couplings and provide a bound on ϕ_h . The authors of [5] used the ATLAS results [66] and concluded that $|\phi_h| < 0.3$. Recent results from the ATLAS experiment are as follows [67]:

$$\frac{g_{WWh}}{g_{WWh}^{\text{SM}}} = 1.035 \pm 0.031, \quad (2.29)$$

$$\frac{g_{ffh}}{g_{ffh}^{\text{SM}}} = 0.95 \pm 0.05, \quad (2.30)$$

with a positive correlation of 39%. Here, g_{ffh} is the h coupling to the SM fermions. Using this constraint on the couplings, we obtain $|\phi_h| < 0.24$. Another constraint comes from the perturbative unitarity bounds on the scalar quartic couplings. It has been found that $|\phi_h| \lesssim 0.1$ [5]. Hence, small $|\phi_h|$ is required from both the experimental and theoretical bounds. Furthermore, DM direct detection experiments provide bounds on ϕ_h . DM candidate V^0 scatters off the nuclei by exchanging scalar bosons in t -channel. The scattering cross section is proportional to $\sin^2 2\phi_h$. The current upper bound on the cross section requires $|\phi_h| \lesssim \mathcal{O}(0.1)$. The XENONnT experiment [68] can cover the region of parameter space for $|\phi_h| \gtrsim \mathcal{O}(0.01)$ in the future [5].

We focus on $|\phi_h| < \mathcal{O}(0.01)$, where both the theoretical and experimental bounds are absent. Direct detection experiments cannot probe the model with such a small $|\phi_h|$ value in the near future. Hence, other experiments, such as GW searches, are useful for examining the model. In the following analysis, we set $\phi_h = 0$ as an approximation of a small ϕ_h value.

Searches for heavy-vector bosons using collider experiments also present some constraints. In this model, W' couples to an SM fermion, and its coupling is described as follows:

$$g_{W'ff} \simeq -\sqrt{\frac{m_{Z'}^2}{m_V^2} - 1} g_{Wff}^{\text{SM}}, \quad (2.31)$$

where g_{Wff}^{SM} is the W coupling to the fermions in the SM. Owing to this coupling, W' can be produced in pp collision. ATLAS and CMS experiments provide stringent bounds

on W' from $pp \rightarrow W' \rightarrow l\nu$. It is found that $m_{W'} \gtrsim 7$ TeV for $m_{V^0} \lesssim 4$ TeV [5]. For $m_{V^0} \gtrsim 4$ TeV, the constraint on $m_{Z'}$ is weaker and negligible. In the future, HL-LHC will be used to search for $m_{Z'} \lesssim 8.5$ TeV if $m_{V^0} \lesssim 5.5$ TeV. We use these bounds and discuss future prospects in Section 5.

3 Loop and finite temperature corrections to scalar potential and phase transition

In this section, the phase transitions of the scalar potential are discussed. We calculate the finite-temperature effective potential and obtain the conditions necessary for the first-order phase transition.

There are two distinct energy scales: the electroweak scale denoted as v , and the scale characterizing the dark sector, represented as v_Φ . As discussed in Section 2, the two scales are well separated, $v_\Phi \gg v$. Consequently, the phase transition within the dark sector precedes the electroweak phase transition. During this transition within the dark sector, electroweak symmetry is restored. This clear separation of the two scales allows us to discuss the two phase transitions separately.

The phase transition in the dark sector can be first-order because the typical values of g_0 and g_1 are $\mathcal{O}(1)$ in a large region of the parameter space [5] and provide sizable corrections to the scalar potential. In the following, we focus on phase transition in the dark sector.

However, the phase transition in the electroweak sector is expected to be the same as that in the SM, which is not first-order. Because the two scales are well separated, $v_\Phi \gg v$, the electroweak phase transition can be discussed using an effective theory in which all the new fields are integrated out, and the Lagrangian is provided by the SM together with higher dimensional operators. In this case, a first-order electroweak phase transition occurs if the energy scale of the new physics is $\mathcal{O}(100)$ GeV [69, 70]. However, the energy scale of the new physics in this model is much higher than the electroweak scale, $v_\Phi \sim \mathcal{O}(1)$ TeV. Therefore, the electroweak phase transition in this model is not first-order; thus, we do not further investigate it in this paper.

3.1 Effective potential

During the phase transition in the dark sector, the electroweak symmetry is well restored, as discussed at the beginning of this section, and the classical background fields of the scalar fields are expressed as

$$\langle \Phi_i \rangle_{cl} = \frac{1}{\sqrt{2}} \begin{pmatrix} \varphi_i & 0 \\ 0 & \varphi_i \end{pmatrix}, \quad \langle H \rangle_{cl} = \begin{pmatrix} 0 \\ 0 \end{pmatrix}, \quad (3.1)$$

where $i = 1, 2$. Linear combinations of φ_1 and φ_2 are used. $\varphi_{h'}$ and φ_{h_D} are defined as follows:

$$\varphi_{h'} = \frac{1}{\sqrt{2}} (\varphi_1 + \varphi_2), \quad \varphi_{h_D} = \frac{1}{\sqrt{2}} (\varphi_1 - \varphi_2). \quad (3.2)$$

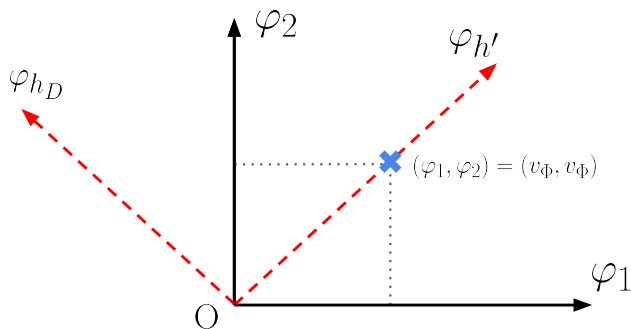


Figure 1. The solid black axes represent the values of the classical fields $\Phi_{1,2}$, whereas the red dashed axes represent h' and h_D . The true vacuum, which corresponds to $\varphi_1 = \varphi_2 = v_\Phi$, is indicated by the blue cross mark.

They correspond to the classical fields of h' and h_D described in Eq. (2.12) and shown in Fig. 1.

The effective potential at the one-loop level, including thermal corrections, can be expressed as

$$V_{\text{eff}}(\varphi_{h'}, \varphi_{h_D}, T) = m_\Phi^2(\varphi_{h'}^2 + \varphi_{h_D}^2) + \frac{\lambda_\Phi}{2}(\varphi_{h'}^4 + 6\varphi_{h'}^2\varphi_{h_D}^2 + \varphi_{h_D}^4) + \frac{\lambda_{12}}{4}(\varphi_{h'}^2 - \varphi_{h_D}^2)^2 + V_{\text{CW}}(\varphi_{h'}, \varphi_{h_D}) + \Delta V_T(\varphi_{h'}, \varphi_{h_D}, T) + \delta V(\varphi_{h'}, \varphi_{h_D}), \quad (3.3)$$

where V_{CW} represents the Coleman-Weinberg potential at the one-loop level, $\Delta V_T(\varphi_{h'}, \varphi_{h_D}, T)$ denotes the thermal correction, and δV contains counterterms that cancel UV divergence.

To evaluate V_{eff} , we must expand the fields around the classical background fields and obtain the field-dependent masses, denoted as \bar{m}_j^2 . The mass terms of the fluctuation fields are expressed as follows¹:

$$\mathcal{L} \supset -\frac{1}{2}(\bar{h}_1 \ \bar{h}_2) \bar{\mathcal{M}}_s^2 \begin{pmatrix} \bar{h}_1 \\ \bar{h}_2 \end{pmatrix} - \frac{1}{2} \sum_{i=1}^2 \sum_{a=1}^3 \bar{m}_{\pi_i}^2 (\bar{\pi}_i^a)^2 + \frac{1}{2} \sum_{a=1}^3 (\bar{W}_0^a \ \bar{W}_1^a \ \bar{W}_2^a) \bar{\mathcal{M}}_G^2 \begin{pmatrix} \bar{W}_0^a \\ \bar{W}_1^a \\ \bar{W}_2^a \end{pmatrix}, \quad (3.4)$$

¹As elucidated in Section 2, we focus on $|\phi_h| < \mathcal{O}(0.01)$ and set $\phi_h \simeq 0$. At this limit, $\lambda_{h\Phi}$ vanishes and does not appear here. As discussed later in this paper, essential contributions are from the gauge couplings, and thus, the results are not significantly modified even if $\lambda_{h\Phi}$ is considered in the effective potential.

where

$$\overline{m}_{\pi_1}^2 = 2m_\Phi^2 + 4\lambda_\Phi\varphi_1^2 + 2\lambda_{12}\varphi_2^2, \quad (3.5)$$

$$\overline{m}_{\pi_2}^2 = 2m_\Phi^2 + 2\lambda_{12}\varphi_1^2 + 4\lambda_\Phi\varphi_2^2, \quad (3.6)$$

$$\overline{\mathcal{M}}_s^2 = \begin{pmatrix} 2m_\Phi^2 + 12\lambda_\Phi\varphi_1^2 + 2\lambda_{12}\varphi_2^2 & 4\lambda_{12}\varphi_1\varphi_2 \\ 4\lambda_{12}\varphi_1\varphi_2 & 2m_\Phi^2 + 12\lambda_\Phi\varphi_2^2 + 2\lambda_{12}\varphi_1^2 \end{pmatrix}, \quad (3.7)$$

$$\overline{\mathcal{M}}_G^2 = \frac{1}{4} \begin{pmatrix} g_0^2\varphi_1^2 & -g_0g_1\varphi_1^2 & 0 \\ -g_0g_1\varphi_1^2 & g_1^2(\varphi_1^2 + \varphi_2^2) & -g_1g_0\varphi_2^2 \\ 0 & -g_1g_0\varphi_2^2 & g_0^2\varphi_2^2 \end{pmatrix}. \quad (3.8)$$

We obtain the eigenvalues of $\overline{\mathcal{M}}_s^2$ as follows:

$$\overline{m}_{h'} = 2m_\Phi^2 + (\lambda_{12} + 6\lambda_\Phi)(\varphi_1^2 + \varphi_2^2) - \sqrt{(\lambda_{12} + 6\lambda_\Phi)^2(\varphi_1^2 - \varphi_2^2)^2 + 16\lambda_{12}^2\varphi_1^2\varphi_2^2}, \quad (3.9)$$

$$\overline{m}_{h_D} = 2m_\Phi^2 + (\lambda_{12} + 6\lambda_\Phi)(\varphi_1^2 + \varphi_2^2) + \sqrt{(\lambda_{12} + 6\lambda_\Phi)^2(\varphi_1^2 - \varphi_2^2)^2 + 16\lambda_{12}^2\varphi_1^2\varphi_2^2}, \quad (3.10)$$

and the eigenvalues of $\overline{\mathcal{M}}_G^2$ as follows:

$$\overline{m}_W^2 = 0, \quad (3.11)$$

$$\overline{m}_V^2 = \frac{g_0^2 + g_1^2}{8}(\varphi_1^2 + \varphi_2^2) - \frac{1}{8}\sqrt{(g_0^2 + g_1^2)^2(\varphi_1^2 - \varphi_2^2)^2 + 4g_1^4\varphi_1^2\varphi_2^2}, \quad (3.12)$$

$$\overline{m}_{Z'}^2 = \frac{g_0^2 + g_1^2}{8}(\varphi_1^2 + \varphi_2^2) + \frac{1}{8}\sqrt{(g_0^2 + g_1^2)^2(\varphi_1^2 - \varphi_2^2)^2 + 4g_1^4\varphi_1^2\varphi_2^2}. \quad (3.13)$$

Using these field-dependent masses, we obtain the following:

$$V_{\text{CW}} = \frac{1}{64\pi^2} \sum_j n_j \overline{m}_j^4 \left(\log \frac{\overline{m}_j^2}{\mu^2} - c_j - \frac{1}{\bar{\epsilon}} \right), \quad (3.14)$$

where $1/\bar{\epsilon}$ represents UV divergence, $c_j = \frac{3}{2} (\frac{5}{6})$ for the scalar (gauge) bosons, μ is a renormalization scale, the summation is taken for the particles coupling to Φ_1 or Φ_2 ($j = \pi_1, \pi_2, h', h_D, W, V$, and Z'), and n_j represents the degrees of freedom of the particles:

$$\begin{aligned} n_{\pi_1} &= n_{\pi_2} = 3, \\ n_{h'} &= n_{h_D} = 1, \\ n_W &= n_V = n_{Z'} = 9. \end{aligned} \quad (3.15)$$

We use $\mu = m_V$ in the following analysis. The counterterms are described as follows:

$$\delta V = \delta\Lambda + \delta m_\Phi^2(\varphi_{h'}^2 + \varphi_{h_D}^2) + \frac{\delta\lambda_\Phi}{2}(\varphi_{h'}^4 + 6\varphi_{h'}^2\varphi_{h_D}^2 + \varphi_{h_D}^4) + \frac{\delta\lambda_{12}}{4}(\varphi_{h'}^2 - \varphi_{h_D}^2)^2, \quad (3.16)$$

where $\delta\Lambda$, δm_Φ^2 , $\delta\lambda_\Phi$, and $\delta\Lambda$ are determined using the following renormalization conditions [71, 72]:²

$$V_{\text{eff.}}|_{\varphi_{h'}=\varphi_{h_D}=0} = 0, \quad (3.17)$$

$$\left. \frac{\partial V_{\text{eff}}}{\partial \varphi_{h'}} \right|_{\varphi_{h'}=\sqrt{2}v_\Phi, \varphi_{h_D}=0} = 0, \quad (3.18)$$

$$\left. \frac{\partial^2 V_{\text{eff}}}{\partial \varphi_{h'}^2} \right|_{\varphi_{h'}=\sqrt{2}v_\Phi, \varphi_{h_D}=0} = m_{h'}^2 - \Delta\Sigma_{h'h'}, \quad (3.19)$$

$$\left. \frac{\partial^2 V_{\text{eff}}}{\partial \varphi_{h_D}^2} \right|_{\varphi_{h'}=\sqrt{2}v_\Phi, \varphi_{h_D}=0} = m_{h_D}^2 - \Delta\Sigma_{h_D h_D}, \quad (3.20)$$

where $m_{h'}$ and m_{h_D} are the pole masses for h' and h_D , respectively, $\Delta\Sigma_{ii} = \Sigma_{ii}(p^2 = m_i^2) - \Sigma_{ii}(p^2 = 0)$, and $\Sigma_{ii}(p^2)$ is the two-point function of h' and h_D . These are evaluated using `FeynArts`, `FormCalc`, and `LoopTools` [73, 74]. The field-independent divergent terms in V_{eff} are absorbed using Eq. (3.17). The result is slightly lengthy and is presented in Appendix B.

The thermal loop correction ΔV_T is expressed as follows [75]:

$$\Delta V_T = \frac{T^4}{2\pi^2} \left\{ \sum_j n_j \int_0^\infty dx x^2 \ln \left[1 - \exp \left(-\sqrt{x^2 + a_j^2} \right) \right] \right\}, \quad (3.21)$$

where $a_j^2 = \frac{\overline{m}_j^2}{T^2}$. It is noteworthy that the SM fermions do not contribute to the effective potential of the dark sector.

The thermal loop calculations result in IR divergences. To avoid this, we replace the field-dependent masses in the effective potential with the following [76, 77]:

$$\overline{m}_{\pi_{1,2}}^2 \rightarrow \overline{m}_{\pi_{1,2}}^2 + T^2 \left(2\lambda_\Phi + \frac{2\lambda_{12}}{3} + \frac{3(g_0^2 + g_1^2)}{16} \right), \quad (3.22)$$

$$\overline{m}_{h',h_D}^2 \rightarrow \overline{m}_{h',h_D}^2 + T^2 \left(2\lambda_\Phi + \frac{2\lambda_{12}}{3} + \frac{3(g_0^2 + g_1^2)}{16} \right), \quad (3.23)$$

$$\overline{\mathcal{M}}_G^2 \rightarrow \overline{\mathcal{M}}_G^2 + a^{(L)} \begin{pmatrix} \frac{5T^2 g_0^2}{6} & 0 & 0 \\ 0 & \frac{13T^2 g_1^2}{6} & 0 \\ 0 & 0 & \frac{5T^2 g_0^2}{6} \end{pmatrix}, \quad (3.24)$$

where $a^{(L)} = 1$ for the longitudinal mode and $a^{(L)} = 0$ for the transverse mode, respectively.

3.2 First-order phase transition

The temperature-dependence of the effective potential is also investigated. Figure 2 shows the contours of $(V_{\text{eff}}(\varphi_1, \varphi_2, T) - V_{\text{eff}}(0, 0, T))/V_{\text{eff}}(0, 0, T)$ at two different temperatures: $T = 3.0$ and 2.47 TeV. To provide an illustrative example, we choose $m_{Z'} = 5.0$ TeV,

²Hereafter, we focus only on the real part of the effective potential.

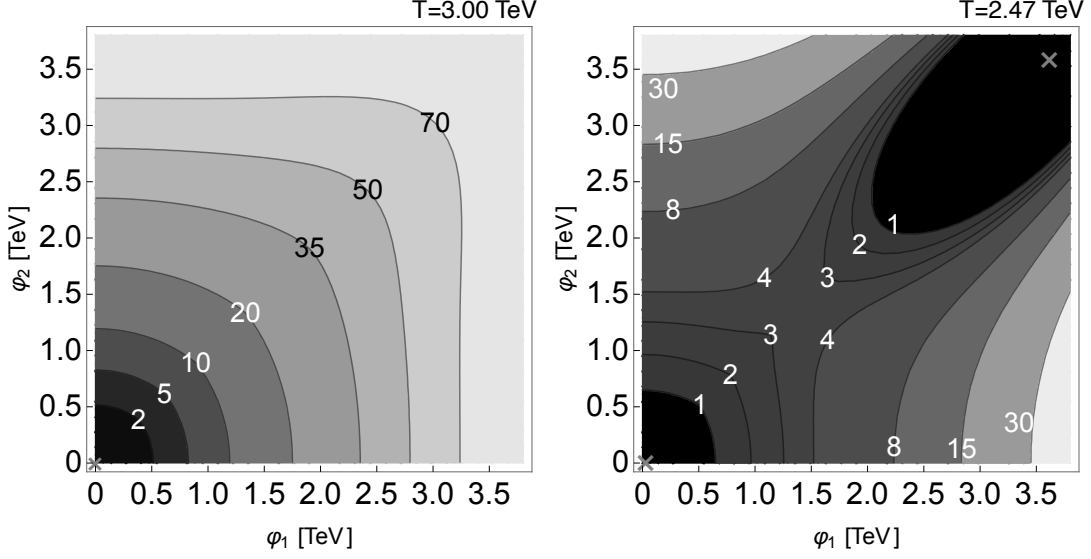


Figure 2. Contours of $(V_{\text{eff}}(\varphi_1, \varphi_2, T) - V_{\text{eff}}(0, 0, T))/V_{\text{eff}}(0, 0, T)$ with $m_{Z'} = 5.0$ TeV, $m_V = 3$ TeV, $m_{h'} = 0.7m_V$, and $m_{h_D} = 1.2m_V$ at $T = 3.0$ and 2.47 TeV. The horizontal and vertical axes are the φ_1 and φ_2 axes, respectively. Darker regions correspond to lower potential values. The cross marks denote the locations of the global minima. At $T = 2.47$ TeV, there are two degenerate minima at the origin and at $\varphi_1 = \varphi_2 \simeq 2$ TeV.

$m_V = 3$ TeV, $m_{h'} = 0.7m_V$, and $m_{h_D} = 1.2m_V$. In this figure, the darker regions correspond to lower potential values. At $T = 3.0$ TeV, the potential has only one minimum, that is, at $\varphi_1 = \varphi_2 = 0$, and thus the symmetry is restored. At $T = 2.47$ TeV, there are two minima. One is at the origin, and the other is at $\varphi_1 = \varphi_2 \simeq 2$ TeV. The two minima have the same potential energies but are separated. Below this temperature, the potential has only one global minimum, that is, at $\varphi_1 = \varphi_2 \neq 0$. Therefore, the potential undergoes a first-order phase transition. The critical temperature (T_C) is the temperature at which the potential has two separate minima. In the example, $T_C = 2.47$ TeV. We also observe that the potential minimum appears along line $\varphi_1 = \varphi_2$. The phase transition also occurs along this line in other parameter choices.

We define φ_C by the value of $\sqrt{\varphi_1^2 + \varphi_2^2}$ at $T = T_C$ and evaluate φ_C/T_C . As we discuss in Section 5, $\varphi_C/T_C \gtrsim 1$ is necessary to produce detectable GW spectra. Figure 3 shows the values of the gauge couplings and φ_C/T_C as functions of $m_{Z'}$. We assign $m_V = 3$ TeV, $m_{h_D} = 1.2m_V$, and $m_{h'}/m_V = 0.7$. The values of the gauge couplings are evaluated by using Eqs. (A.12) and (A.13). This figure shows that an increase in the gauge couplings g_0 and g_1 facilitates a first-order phase transition and leads to an increase in the φ_C/T_C value. The values of these gauge couplings are relatively large for obtaining the measured value of the DM energy density [5]. Consequently, the model realizes a first-order phase transition over a broad range of parameter space.

The value of φ_C/T_C also depends on $m_{h'}$. Figure 4 shows the values of φ_C/T_C in the $m_{h'}-m_{Z'}$ plane for $m_V = 3, 5,$ and 7 TeV. We set $m_{h_D} = 1.2m_V$ in all three panels. The black dashed lines represent $\Omega h^2 = 0.12$. The value of φ_C/T_C decreases for a larger $m_{h'}$.

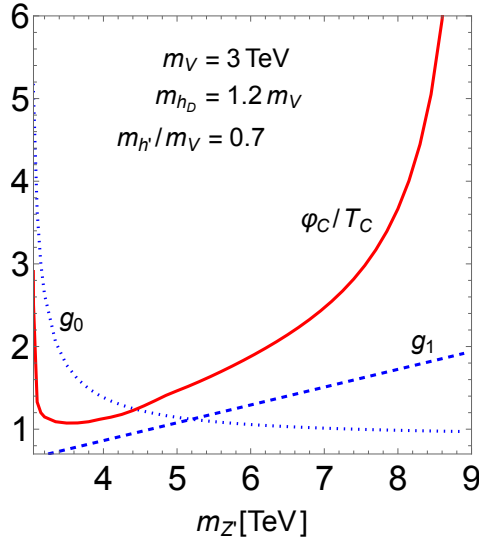


Figure 3. Values of g_0 , g_1 , and φ_C/T_C for $m_V = 3$ TeV, $m_{h_D} = 1.2m_V$, and $m_{h'}/m_V = 0.7$. The blue dotted curve, blue dashed lines, and red solid curve indicate the values of g_0 , g_1 , and φ_C/T_C , respectively.

regime. In the regions to the left of the thick black lines, the vacuum expectation value remains zero, even in the current universe. The φ_C/T_C values are larger for smaller $m_{h'}$ regions because, for small φ , the effective potential at $T = 0$ under the renormalization conditions described in Eqs. (3.17)–(3.20) are expressed as

$$V_{\text{CW}} + \delta V \simeq -\frac{1}{4} \left(m_{h'}^2 - \frac{9(m_V^4 + m_{Z'}^4)}{16\pi^2 v_\Phi^2} \right) \varphi^2 \quad (\text{for small } \varphi), \quad (3.25)$$

where $\varphi = \sqrt{\varphi_1^2 + \varphi_2^2}$. The coefficient is negative at the tree level but can be positive at the loop level because of gauge boson contributions. If it is positive, a local minimum is generated at $\varphi = 0$ even at the tree level. In other words, a potential barrier is generated at the tree level; thus, a first-order phase transition occurs at a lower temperature. This is why φ_C/T_C values are larger for smaller $m_{h'}$ values. We also find that the difference between the two local minima can be approximately described as

$$V_{\text{eff}} \Big|_{\varphi=\sqrt{2}v_\Phi, T=0} - V_{\text{eff}} \Big|_{\varphi=0, T=0} \simeq -\frac{v_\Phi^2}{4} \left(m_{h'}^2 - \frac{9(m_V^4 + m_{Z'}^4)}{32\pi^2 v_\Phi^2} \right). \quad (3.26)$$

If this value is positive, the vacuum at $\varphi = 0$ is the global minimum at $T = 0$. Subsequently, a first-order phase transition does not occur; hence, thick black lines appear in Fig. 4. Even if Eq. (3.26) is negative, namely the vacuum at $\varphi \neq 0$ is the global minimum, φ may persist zero if a tunneling rate is low, as we discuss in Section 4. This is another reason for the thick black lines.

4 Gravitational wave spectrum

We use the GW observational experiments to explore the model parameter space in which a strong first-order phase transition occurs. Before discussing the testability of the model

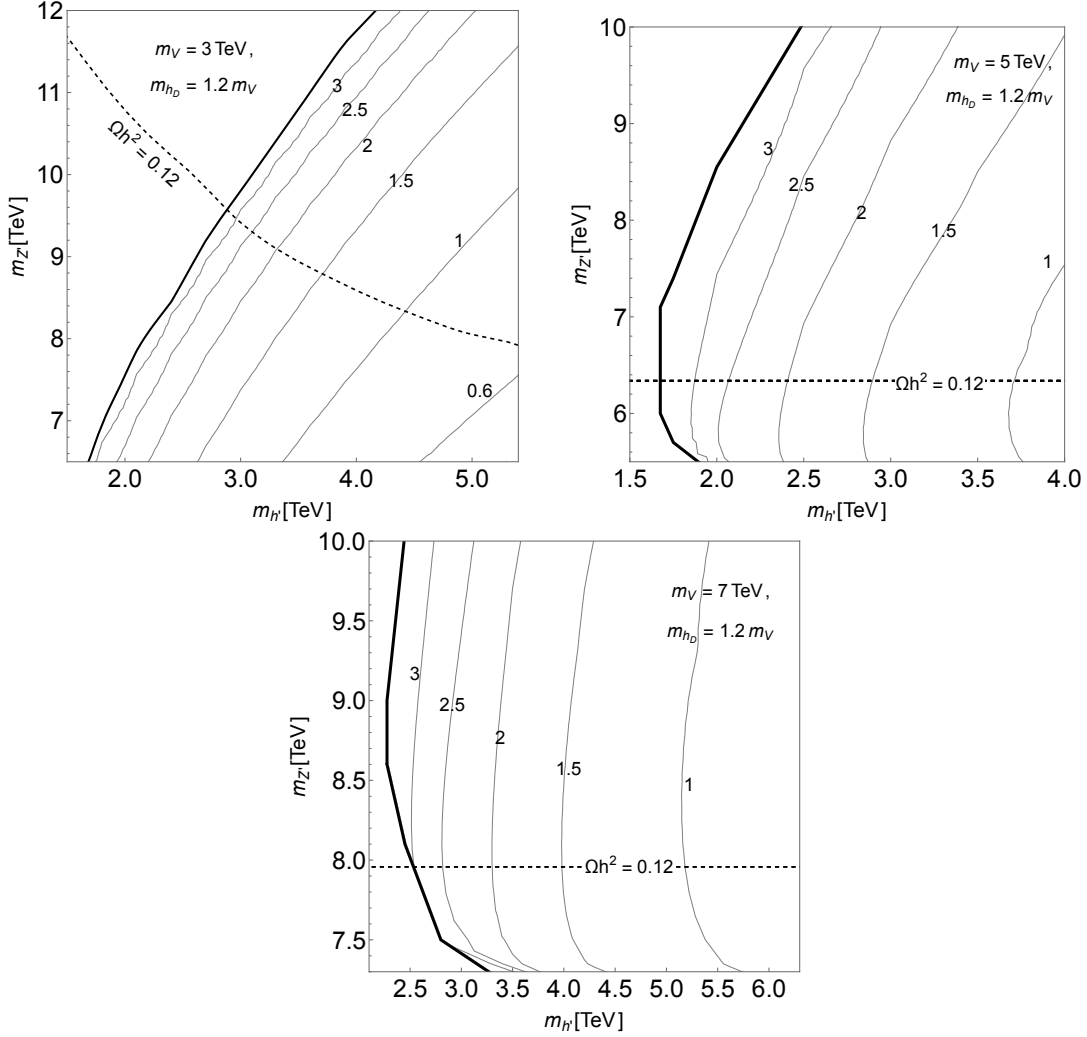


Figure 4. Values of φ_C/T_C in the $m_{h'}$ - $m_{Z'}$ plane with $m_V = 3, 5$ and 7 TeV and $m_{h_D} = 1.2m_V$. The upper left (right) panel shows the value of φ_C/T_C for $m_V = 3$ (5) TeV. The lower panel shows the value for $m_V = 7$ TeV. The black dashed lines represent $\Omega h^2 = 0.12$. The vacuum expectation value remains zero in the regions to the left of the thick-black lines, even in the current universe.

through GW, we briefly introduce herein the evolution of the GW spectrum from the first-order phase transition, which is characterized by (i) nucleation temperature T_n , (ii) α , which is a parameter related to the latent heat, (iii) β , the inverse of the duration of the phase transition, and (iv) a bubble wall velocity v_b .

The nucleation temperature T_n is determined using the following:

$$\left. \frac{\Gamma}{H^4} \right|_{T=T_n} = 1, \quad (4.1)$$

where H is the Hubble parameter, and Γ is the critical bubble nucleation rate per unit

volume per unit time defined as [78]

$$\Gamma(T) \simeq T^4 \left(\frac{S_3}{2\pi T} \right)^{\frac{3}{2}} \exp(-S_3/T), \quad (4.2)$$

where S_3 is a three-dimensional Euclidean action [79]. It is expressed as

$$S_3 = \int d^3r \left[\frac{1}{2} (\vec{\nabla} \varphi_b)^2 + V_{\text{eff}}(\varphi_b, T) \right], \quad (4.3)$$

where φ_b is the bounce solution. It is obtained by solving the following differential equation:

$$\frac{d^2\varphi}{dr^2} + \frac{2}{r} \frac{d\varphi}{dr} - \frac{\partial V_{\text{eff}}}{\partial \varphi} = 0, \quad (4.4)$$

with the following boundary conditions:

$$\left. \frac{d\varphi}{dr} \right|_{r=0} = 0, \quad \lim_{r \rightarrow \infty} \varphi = 0. \quad (4.5)$$

If $\Gamma/H^4 < 1$ today, the phase transition would not be completed even in the current universe. This inconsistency necessitates that Γ/H^4 must have reached one before today. We calculate the Hubble parameter using $H = 8\pi^3 g_* T^4 / 90 m_{\text{Pl}}^2$, where m_{Pl} is the Planck mass, and g_* is the degrees of freedom in the plasma.

The second parameter, denoted as α , represents the released latent heat normalized by the radiative energy density, $\rho_{\text{rad}}(T) = (\pi^2/30)g_*T^4$ at the nucleation temperature T_n . It is defined as

$$\alpha = \epsilon(T_n) / \rho_{\text{rad}}(T_n), \quad (4.6)$$

where $\epsilon(T)$ represents the released latent heat and is defined as

$$\epsilon(T) = \Delta V_{\text{eff}} - T \frac{\partial \Delta V_{\text{eff}}}{\partial T}, \quad (4.7)$$

with

$$\Delta V_{\text{eff}} = V_{\text{eff}}(\varphi_-(T), T) - V_{\text{eff}}(\varphi_+(T), T). \quad (4.8)$$

Here, φ_+ and φ_- are the order parameters for the broken and unbroken phases, respectively.

The third parameter, denoted as β/H , represents the inverse of the duration of the phase transition. It is expressed as

$$\frac{\beta}{H} \equiv T_n \left. \frac{d}{dT} \left(\frac{S_3}{T} \right) \right|_{T=T_n}. \quad (4.9)$$

The fourth parameter, v_b , is the bubble-wall velocity in the rest frame of the plasma far from the wall. We choose $v_b = 0.3$ and 1 as benchmark points in our numerical analysis.³

³There is no easy way to estimate bubble wall velocity; however, the authors of [80] have recently proposed a formula to estimate terminal wall velocity for strongly coupled first-order phase transition. Therefore, it is generally better to consider velocity as a free parameter, and we use $v_b = 0.3$ and 1 as benchmark points in our analysis.

The first-order phase transition generates GWs through three mechanisms: bubble collision, plasma turbulence, and compression waves in the plasma. The contribution of bubble wall collisions becomes significant when the bubble walls accelerate rapidly [81]. However, runaway bubble wall expansion is unlikely [82]. The contribution of the turbulence is described in [83, 84]. However, it is generally subdominant. In the following analysis, we consider the GW from the compression wave. The fitting function for the numerical simulations of the GW spectrum is expressed as [85, 86]

$$\Omega_{\text{GW}}(f) = 2.061 F_{\text{gw},0} \tilde{\Omega}_{\text{gw}} \left(\frac{f}{\tilde{f}_{\text{comp}}} \right)^3 \left(\frac{7}{4 + 3(f/\tilde{f}_{\text{comp}})^2} \right)^{7/2} \times \begin{cases} \left(\frac{\kappa_v \alpha}{1 + \alpha} \right)^2 (H_* R_*) & (H_* R_* \leq \sqrt{\frac{3}{4} \kappa_v \alpha / (1 + \alpha)}) \\ \left(\frac{\kappa_v \alpha}{1 + \alpha} \right)^{3/2} (H_* R_*)^2 & (\sqrt{\frac{3}{4} \kappa_v \alpha / (1 + \alpha)} < H_* R_*) \end{cases}, \quad (4.10)$$

where $F_{\text{gw},0} = 3.57 \times 10^{-5} (100/g_*)^{1/3}$, $\tilde{\Omega}_{\text{gw}} = 1.2 \times 10^{-2}$, $H_* R_* = (8\pi)^{1/3} (\beta/H)^{-1} \max(c_s, v_b)$, and \tilde{f}_{comp} is the peak frequency expressed as

$$\tilde{f}_{\text{comp}} \simeq 0.26 (H_* R_*)^{-1} \left(\frac{T_n}{\text{GeV}} \right) \left(\frac{g_*}{100} \right)^{1/6} \text{ Hz}. \quad (4.11)$$

In addition, κ_v in the fitting function is an efficiency factor [87]:

$$\kappa_v(v_b, \alpha) \simeq \begin{cases} \frac{c_s^{11/5} \kappa_A \kappa_B}{(c_s^{11/5} - v_b^{11/5}) \kappa_B + v_b c_s^{6/5} \kappa_A} & (v_b \lesssim c_s) \\ \kappa_B + (v_b - c_s) \delta \kappa + \frac{(v_b - c_s)^3}{(v_J - c_s)^3} [\kappa_C - \kappa_B - (v_J - c_s) \delta \kappa] & (c_s < v_b < v_J) \\ \frac{(v_J - 1)^3 v_J^{5/2} v_b^{-5/2} \kappa_C \kappa_D}{[(v_J - 1)^3 - (v_b - 1)^3] v_J^{5/2} \kappa_C + (v_b - 1)^3 \kappa_D} & (v_J \lesssim v_b) \end{cases}, \quad (4.12)$$

where $c_s = 0.577$, and

$$\kappa_A \simeq v_b^{6/5} \frac{6.9\alpha}{1.36 - 0.037\sqrt{\alpha} + \alpha}, \quad (4.13)$$

$$\kappa_B \simeq \frac{\alpha^{2/5}}{0.017 + (0.997 + \alpha)^{2/5}}, \quad (4.14)$$

$$\kappa_C \simeq \frac{\sqrt{\alpha}}{0.135 + \sqrt{0.98 + \alpha}}, \quad (4.15)$$

$$\kappa_D \simeq \frac{\alpha}{0.73 + 0.083\sqrt{\alpha} + \alpha}, \quad (4.16)$$

$$v_J = \frac{\sqrt{2/3\alpha + \alpha^2} + \sqrt{1/3}}{1 + \alpha}, \quad (4.17)$$

$$\delta \kappa \simeq -0.9 \ln \frac{\sqrt{\alpha}}{1 + \sqrt{\alpha}}. \quad (4.18)$$

Using these equations, the GW spectrum of the first-order phase transition is evaluated. To discuss the detail of the testability of the model using the GW spectrum, we use the

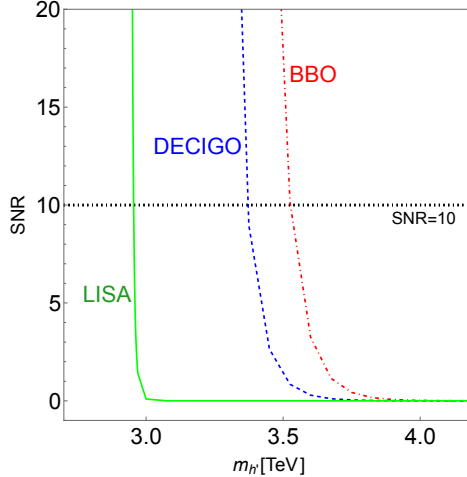


Figure 5. The value of SNR for $m_V = 3$ TeV as a function of $m_{h'}$. Other parameters are $m_{h_D} = 1.2m_V$, $v_b = 0.3$, and $\mathcal{T} = 4$ yrs. The $m_{Z'}$ is adapted to explain the DM energy $\Omega h^2 = 0.12$. The green solid, blue dashed, and red dot-dashed lines represent the SNR values with $\mathcal{T} = 4$ yrs and $v_b = 0.3$ in the LISA, DECIGO, and BBO experiments, respectively. The black horizontal dotted line represents SNR = 10.

signal-to-noise ratio (SNR) [88], which is expressed as

$$\text{SNR} = \sqrt{\mathcal{T} \int_{f_{\min}}^{f_{\max}} df \left[\frac{h^2 \Omega_{\text{GW}}(f)}{h^2 \Omega_{\text{sen}}(f)} \right]^2}, \quad (4.19)$$

where \mathcal{T} is the experimental period, and $h^2 \Omega_{\text{sen}}(f)$ is a sensitivity curve of a GW detector. Three future GW experiments are considered: LISA, DECIGO, and BBO [89, 90]. A GW spectrum with SNR > 10 can be used to explore the model parameters [70, 91]. We use this criterion to discuss the testability of the GW observations in our numerical analysis.

5 Results

We investigate the parameter regions that can explain the DM energy density, which can be explored through collider experiments and GW observations.

Figure 5 shows the SNR values for $m_V = 3$ TeV in the LISA, DECIGO, and BBO experiments. The vertical axis represents the SNR value, and the horizontal axis represents the $m_{h'}$. The green solid, blue dashed, and red dotted dashed lines represent the SNR values for the LISA, DECIGO, and BBO experiments, respectively. The black horizontal dotted line represents SNR = 10, and each experiment can test the parameter region to the left of each intersection. Therefore, generating the detectable GW spectra for smaller $m_{h'}$ values is easier. For small $m_{h'}$, the quadratic and quartic terms in the tree-level potential are small. A sizable barrier can be easily generated if these terms are comparable to the cubic term from thermal loop effects, and the φ_C/T_C becomes large. Because the phase transition parameters depend on the value of φ_C/T_C , $\alpha \propto (\varphi_C/T_C)^2$ and $\beta/H \propto (\varphi_C/T_C)^{-5/2}$ [87, 91, 92], detectable GW can be produced for small $m_{h'}$.

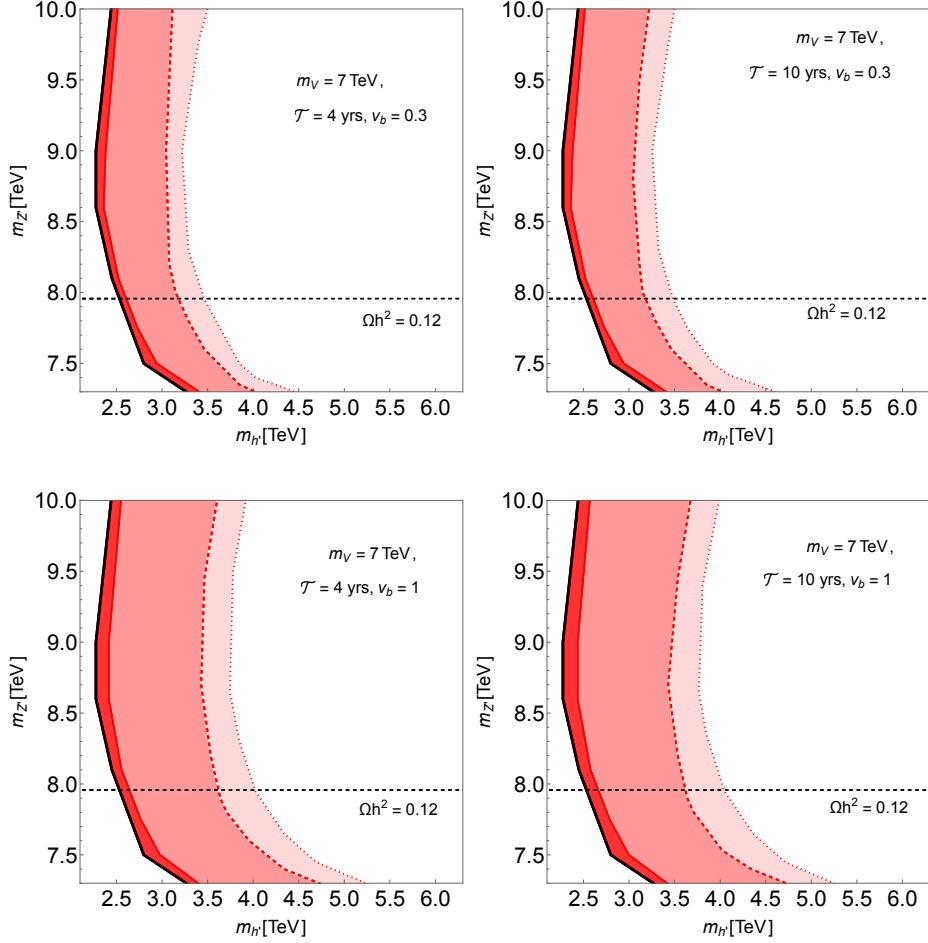


Figure 6. Detectability of the GW in the $m_{h'}$ - $m_{Z'}$ plane for $m_V = 7$ TeV and $m_{h_D} = 1.2m_V$. The upper (lower) two panels are for $v_b = 0.3$ ($v_b = 1$). In the left (right) panels, $\mathcal{T} = 4$ (10) yrs. In the light red regions, $\text{SNR} > 10$ in the BBO, DECIGO, and LISA experiments. In the standard red regions, $\text{SNR} > 10$ in the DECIGO and LISA experiments. In the dark red regions, $\text{SNR} > 10$ only in the LISA experiment. The black dashed lines indicate the regions where the measured value of the DM energy density is explained by the freeze-out mechanism.

Figure 6 shows the region where $\text{SNR} > 10$ in each GW experiment in the $m_{h'}$ - $m_{Z'}$ plane for $m_V = 7$ TeV and $m_{h_D} = 1.2m_V$. The heavy vector and scalar bosons in the parameter region in this figure cannot be explored through the direct W' search in the current and future collider experiments. The upper (lower) two panels correspond to $v_b = 0.3$ ($v_b = 0.1$). Dark red, standard red, and light red represent the regions where the SNR exceeds 10 in each experiment. In the light red region, the SNR is larger than ten in the BBO experiment. In contrast, the standard red (dark red) regions are tested using DECIGO and BBO (LISA, DECIGO, and BBO) experiments. A strong first-order phase transition is not realized in the white regions to the right of the light-red region; thus, detectable GW spectra are not generated. In the regions to the left of the dark red regions, the phase transition is not completed in the current universe, namely $\Gamma/H^4 < 1$. The black dashed lines indicate the

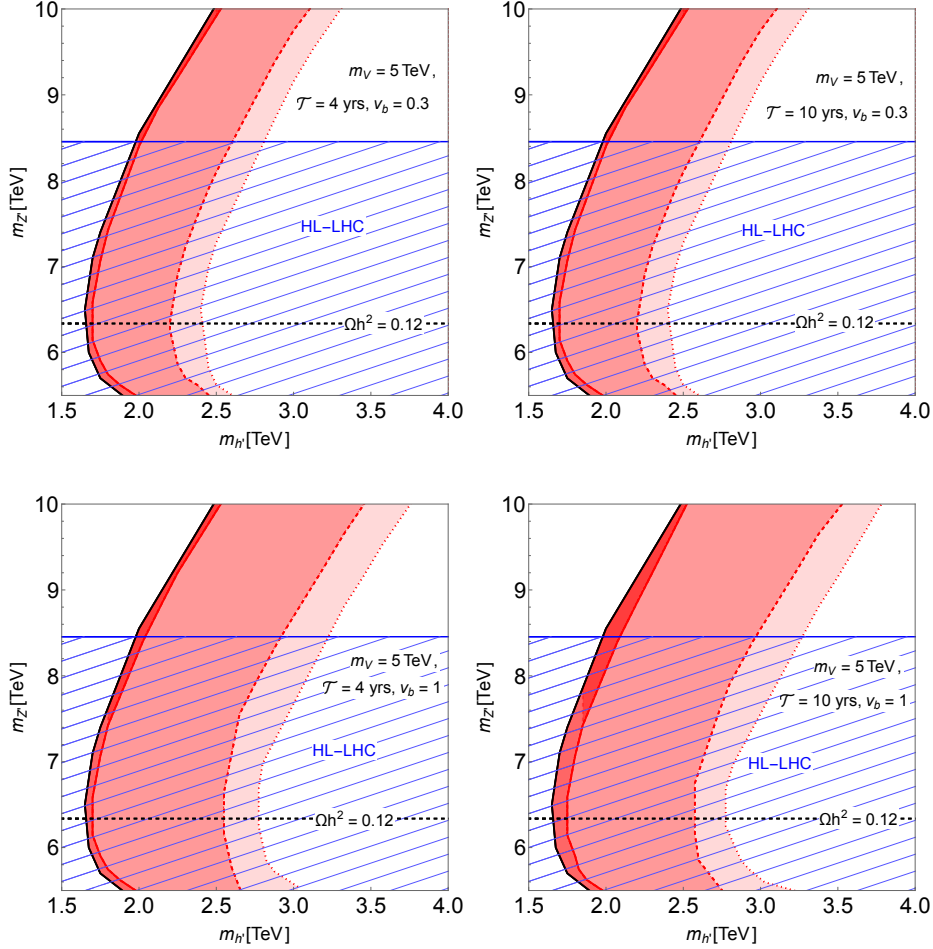


Figure 7. Detectability of the GW for $m_V = 5$ TeV. The blue-hatched regions are explored using the HL-LHC. The other color notations are the same as in Fig. 6.

regions where the measured value of the DM energy density is explained by the freeze-out mechanism. We find that if $m_V = 7$ TeV and $m_{h'}$ is within the range of $2.5 \text{ TeV} \lesssim m_{h'} \lesssim 3.5 \text{ TeV}$, the model can explain the DM energy density and can be tested using the GW observational experiments. It is difficult to produce such a heavy h' in collider experiments. However, we can test the heavy h' regime using the GW signals.

Figure 7 is similar to Fig. 6, except for $m_V = 5$ TeV. The HL-LHC can test the model using the W' search if the model parameters are within the blue-hatched regions. The blue-hatched and red regions are overlapped when $1.6 \text{ TeV} \lesssim m_{h'} \lesssim 2.5 \text{ TeV}$. In this mass range, the model can be tested using both the W' search at the HL-LHC and GW observational experiments. Because it is difficult to produce a heavy h' in collider experiments, the GW signal is a useful tool to determine the value of $m_{h'}$.

For $m_V = 3$ TeV, which is shown in Fig. 8, some regions of the parameter space are excluded by the direct search of W' in the ATLAS experiment. For the parameter points that can explain the measured value of the DM energy density, the HL-LHC is used to test the model for $m_{h'} \gtrsim 4$ TeV, and the GW observational experiments are used for 2.8 TeV

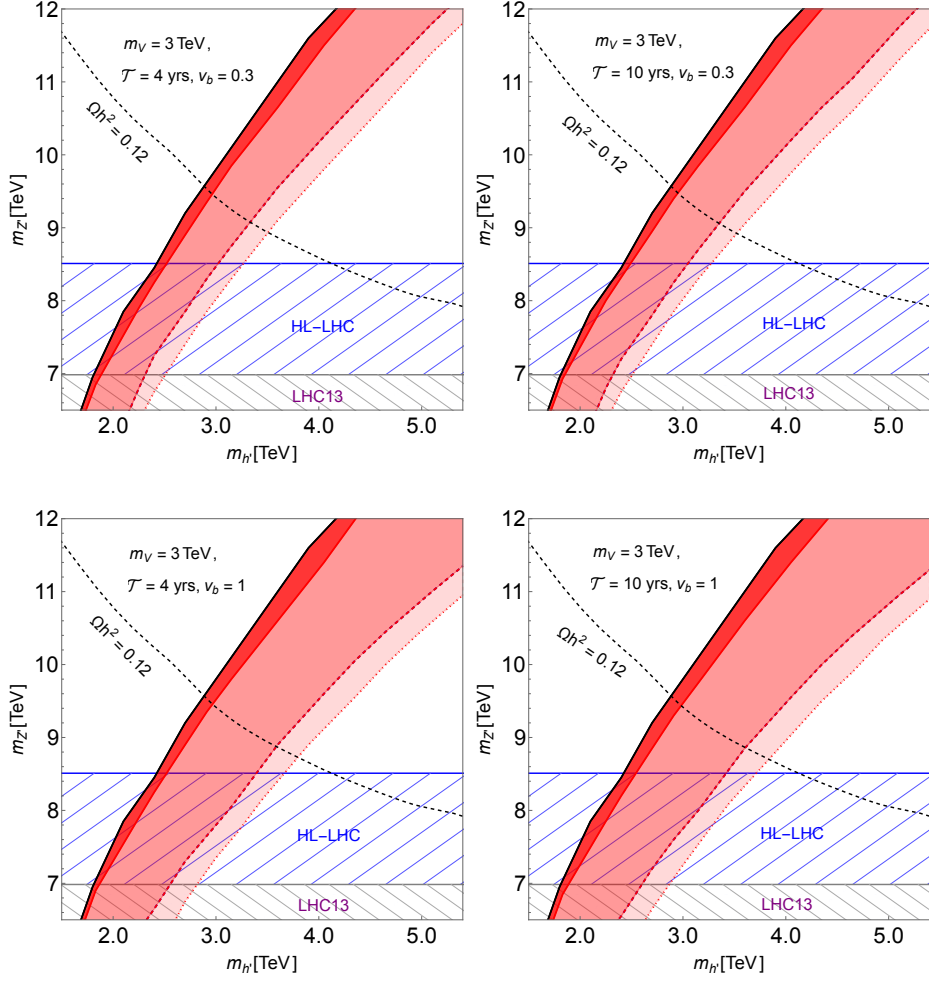


Figure 8. Detectability of the GW for $m_V = 3$ TeV. The W' search at the ATLAS experiment excludes the black-hatched region. The other color notation is the same as in Fig. 6.

$\gtrsim m_{h'} \gtrsim 3.5$ TeV. Therefore, the collider and GW observational experiments complement each other.

6 Conclusion

We have discussed the GWs in an electroweakly interacting vector DM model, which has an extended gauge symmetry: $SU(3)_C \times SU(2)_0 \times SU(2)_1 \times SU(2)_2 \times U(1)_Y$. To ensure the stability of the DM, we assume exchange symmetry between $SU(2)_0$ and $SU(2)_2$, and a new gauge boson V^0 is a DM candidate. Above the electroweak scale, a phase transition $SU(2)_0 \times SU(2)_1 \times SU(2)_2 \rightarrow SU(2)_L$ occurs. All new particles in the model are bosons, and the new gauge couplings can be relatively large within the perturbative regime. Thus, a potential barrier is easily produced during the phase transition. Consequently, the phase transition is strongly first order and produces detectable gravitational waves.

We found that the effective potential with finite temperature is sensitive to $m_{h'}$. When $m_{h'}$ value is large, the corrections by the gauge bosons are relatively smaller than the contribution of $m_{h'}$ at the tree level; thus, the phase transition is not strongly first-order. For smaller $m_{h'}$, the loop effects of the gauge bosons are significant; thus, φ_C/T_C becomes larger. However, when $m_{h'}$ is small, the gauge boson contributions generate a local minimum at the potential origin. For relatively smaller $m_{h'}$, the local minimum at the origin becomes the global minimum of the potential, and the phase transition does not occur. Even when the global minimum is at $\varphi \neq 0$, the tunneling rate is low, and the phase transition does not occur when $m_{h'}$ is small. Therefore, there is a lower bound on $m_{h'}$ for the phase transition.

The model predicts a detectable GW spectrum in the LISA, DECIGO, and BBO experiments. With the assumption that the model explains the measured value of the DM energy density through the freeze-out mechanism, the model predicts detectable GW spectra when $2.5 \text{ TeV} \lesssim m_{h'} \lesssim 3.5 \text{ TeV}$ for $m_V = 7 \text{ TeV}$, $1.6 \text{ TeV} \lesssim m_{h'} \lesssim 2.5 \text{ TeV}$ for $m_V = 5 \text{ TeV}$, and $2.8 \text{ TeV} \lesssim m_{h'} \lesssim 3.5 \text{ TeV}$ for $m_V = 3 \text{ TeV}$. Because it is difficult to produce heavy h' in collider experiments, it is crucial to use GW signals in determining $m_{h'}$.

Acknowledgments

This work was supported by JSPS KAKENHI Grant Number 19H04615 and 21K03549 [T.A.]. We would like to thank Editage (www.editage.jp) for English language editing.

A Approximated expressions of the gauge bosons for $v_\Phi \gg v$

For $v_\Phi \gg v$, the approximate mass eigenstates are described as

$$V_\mu^0 = \frac{W_{0\mu}^3 - W_{2\mu}^3}{\sqrt{2}}, \quad (\text{A.1})$$

$$V_\mu^\pm = \frac{W_{0\mu}^\pm - W_{2\mu}^\pm}{\sqrt{2}}, \quad (\text{A.2})$$

$$Z'_\mu \simeq \frac{g_0}{\sqrt{g_0^2 + 2g_1^2}} \frac{W_{0\mu}^3 + W_{2\mu}^3}{\sqrt{2}} - \frac{\sqrt{2}g_1}{\sqrt{g_0^2 + 2g_1^2}} W_{1\mu}^3, \quad (\text{A.3})$$

$$W_\mu^{\prime\pm} \simeq \frac{m_V}{m_{Z'}} \frac{W_{0\mu}^\pm + W_{2\mu}^\pm}{\sqrt{2}} - \sqrt{1 - \left(\frac{m_V}{m_{Z'}}\right)^2} W_{1\mu}^\pm, \quad (\text{A.4})$$

$$W_\mu^\pm \simeq \sqrt{1 - \left(\frac{m_V}{m_{Z'}}\right)^2} \frac{W_{0\mu}^\pm + W_{2\mu}^\pm}{\sqrt{2}} + \frac{m_V}{m_{Z'}} W_{1\mu}^\pm, \quad (\text{A.5})$$

$$Z_\mu \simeq \frac{eg_1}{\sqrt{g_0^2 + 2g_1^2}g'} (W_{0\mu}^3 + W_{2\mu}^3) + \frac{eg_0}{\sqrt{g_0^2 + 2g_1^2}g'} W_{1\mu}^3 - \frac{e\sqrt{g_0^2 + 2g_1^2}}{g_0g_1} B_\mu, \quad (\text{A.6})$$

$$A_\mu = \frac{e}{g_0} (W_{0\mu}^3 + W_{2\mu}^3) + \frac{e}{g_1} W_{1\mu}^3 + \frac{e}{g'} B_\mu, \quad (\text{A.7})$$

where e is the electric charge, expressed as $e = \sqrt{2/g_0^2 + 1/g_1^2 + 1/g'^2}$. The masses of these gauge bosons at the tree level are described as follows:

$$m_{V^0}^2 = m_{V^\pm}^2 = \frac{g_0^2 v_\Phi^2}{4}, \quad (\text{A.8})$$

$$m_{Z'}^2 \simeq m_{W^{\prime\pm}}^2 \simeq \frac{(g_0^2 + 2g_1^2)v_\Phi^2}{4}, \quad (\text{A.9})$$

$$m_{W^\pm}^2 \simeq \frac{g_0^2 g_1^2 v^2}{4(g_0^2 + 2g_1^2)}, \quad (\text{A.10})$$

$$m_Z^2 \simeq \frac{g_0^2 g_1^2 g'^2 v^2}{4e^2(g_0^2 + 2g_1^2)}. \quad (\text{A.11})$$

At the 1-loop level, the mass difference between V^\pm and V^0 is $m_{V^\pm} - m_{V^0} \simeq 166$ MeV [5]. Using the masses of the gauge bosons, the gauge couplings g_0 and g_1 for $v_\Phi \gg v$ can be expressed as

$$g_0 \simeq \sqrt{2}g_W \frac{m_{Z'}}{m_V} \frac{1}{\sqrt{\frac{m_{Z'}^2}{m_V^2} - 1}} \quad (\text{A.12})$$

$$g_1 \simeq g_W \frac{m_{Z'}}{m_V}, \quad (\text{A.13})$$

where g_W is

$$g_W = \left(\frac{2}{g_2^2} + \frac{1}{g_1^2} \right)^{-1/2}. \quad (\text{A.14})$$

B $V_{\text{CW}} + \delta V$

Defining $\varphi = \sqrt{\varphi_1^2 + \varphi_2^2}$, then the renormalized effective potential at $T = 0$ as a function of φ can be expressed as follows:

$$\begin{aligned}
V_{\text{eff}} \Big|_{T=0} &= \frac{m_{h'}^2 - \Delta \Sigma_{h'h'}}{16v_{\Phi}^2} ((\varphi^2 - 2v_{\Phi}^2)^2 - 4v_{\Phi}^4) \\
&+ 9 \frac{m_V^4}{32\pi^2} \frac{\varphi^2}{2v_{\Phi}^2} + 9 \frac{m_{Z'}^4}{32\pi^2} \frac{\varphi^2}{2v_{\Phi}^2} \\
&+ 9 \frac{m_V^4}{64\pi^2} \frac{\varphi^4}{4v_{\Phi}^4} \left(\ln \frac{\varphi^2}{2v_{\Phi}^2} - \frac{3}{2} \right) + 9 \frac{m_{Z'}^4}{64\pi^2} \frac{\varphi^4}{4v_{\Phi}^4} \left(\ln \frac{\varphi^2}{2v_{\Phi}^2} - \frac{3}{2} \right) \\
&+ \frac{1}{64\pi^2} \langle m_{h'}^2 \rangle^2 \left(\ln \frac{\langle m_{h'}^2 \rangle}{m_{h'}^2} - \frac{3}{2} \right) + \frac{1}{32\pi^2} \langle m_{h'}^2 \rangle m_{h'}^2 \\
&+ \frac{1}{64\pi^2} \langle m_{h_D}^2 \rangle^2 \left(\ln \frac{\langle m_{h_D}^2 \rangle}{m_{h_D}^2} - \frac{3}{2} \right) + \frac{1}{32\pi^2} \langle m_{h_D}^2 \rangle m_{h_D}^2 \\
&- 6 \frac{(\lambda_{12} + 2\lambda_{\Phi})^2}{128\pi^2} 3\varphi^2 (-4v_{\Phi}^2 + \varphi^2) \\
&+ 6 \frac{(\lambda_{12} + 2\lambda_{\Phi})^2 (\varphi^2 - 2v_{\Phi}^2)^2}{64\pi^2} \ln \frac{(\lambda_{12} + 2\lambda_{\Phi})(\varphi^2 - 2v_{\Phi}^2)}{m_G^2} \\
&+ (\varphi\text{-independent terms}), \tag{B.1}
\end{aligned}$$

where

$$m_G^2 = \lim_{\varphi \rightarrow \sqrt{2}v_\Phi} (\varphi^2 - 2v_\Phi^2), \quad (\text{B.2})$$

$$m_\Phi^2 = -v_\Phi^2(\lambda_{12} + 2\lambda_\Phi), \quad (\text{B.3})$$

$$\langle m_{h'}^2 \rangle = -2v_\Phi^2(\lambda_{12} + 2\lambda_\Phi) + (\lambda_{12} - 2\sqrt{\lambda_{12}^2 + 6\lambda_\Phi})\varphi^2, \quad (\text{B.4})$$

$$\langle m_{h_D}^2 \rangle = -2v_\Phi^2(\lambda_{12} + 2\lambda_\Phi) + (\lambda_{12} + 2\sqrt{\lambda_{12}^2 + 6\lambda_\Phi})\varphi^2, \quad (\text{B.5})$$

$$\begin{aligned} \Delta\Sigma_{h'h'} &= \frac{3m_{h'}^2}{32\pi^2 v_\Phi^2} (A_0(m_V^2) + A_0(m_{Z'}^2)) \\ &+ \frac{3m_\Phi^4}{2\pi^2 v_\Phi^2} B_0(0, 0, 0) + \frac{(\lambda_{12} - 6\lambda_\Phi)^2 v_\Phi^2}{4\pi^2} B_0(0, m_{h_D}^2, m_{h_D}^2) \\ &+ \frac{9m_\Phi^4}{4\pi^2 v_\Phi^2} B_0(0, m_{h'}^2, m_{h'}^2) + \frac{9m_V^4}{16\pi^2 v_\Phi^2} B_0(0, m_V^2, m_V^2) \\ &+ \frac{9m_{Z'}^4}{16\pi^2 v_\Phi^2} B_0(0, m_{Z'}^2, m_{Z'}^2) \\ &- \frac{3(-m_{h'}^4 + 16m_\Phi^4)}{32\pi^2 v_\Phi^2} B_0(m_{h'}^2, 0, 0) - \frac{(\lambda_{12} - 6\lambda_\Phi)^2 v_\Phi^2}{4\pi^2} B_0(m_{h'}^2, m_{h_D}^2, m_{h_D}^2) \\ &- \frac{9m_\Phi^4}{4\pi^2 v_\Phi^2} B_0(m_{h'}^2, m_{h'}^2, m_{h'}^2) \\ &- \frac{3(m_{h'}^4 - 4m_{h'}^2 m_V^2 + 12m_V^4)}{64\pi^2 v_\Phi^2} B_0(m_{h'}^2, m_V^2, m_V^2) \\ &- \frac{3(m_{h'}^4 - 4m_{h'}^2 m_{Z'}^2 + 12m_{Z'}^4)}{64\pi^2 v_\Phi^2} B_0(m_{h'}^2, m_{Z'}^2, m_{Z'}^2) \\ &- m_{h'}^2 \delta_Z. \end{aligned} \quad (\text{B.6})$$

Here, δ_Z is the counter term for the wave-function renormalization. When the MS bar scheme is applied, the IR divergences originated from the would-be NG boson contributions in V_{CW} and $\Delta\Sigma$ cancel each other. After the cancelation, the dominant contribution of $\Delta\Sigma$ to the potential comes from the terms depending on the gauge couplings, described as

$$\Delta\Sigma_{h'h'} \simeq \frac{9m_{h'}^2}{32\pi^2 v_\Phi^2} \left(m_V^2 \ln \frac{\mu^2}{m_V^2} + m_{Z'}^2 \ln \frac{\mu^2}{m_{Z'}^2} \right). \quad (\text{B.7})$$

References

- [1] N. Aghanim *et al.* [Planck], *Astron. Astrophys.* **641**, A6 (2020) [erratum: *Astron. Astrophys.* **652**, C4 (2021)] doi:10.1051/0004-6361/201833910 [arXiv:1807.06209 [astro-ph.CO]].
- [2] B. W. Lee and S. Weinberg, *Phys. Rev. Lett.* **39** (1977), 165-168
- [3] J. Hisano, S. Matsumoto, M. Nagai, O. Saito and M. Senami, *Phys. Lett. B* **646** (2007), 34-38 doi:10.1016/j.physletb.2007.01.012 [arXiv:hep-ph/0610249 [hep-ph]].
- [4] M. Cirelli, A. Strumia and M. Tamburini, *Nucl. Phys. B* **787** (2007), 152-175 doi:10.1016/j.nuclphysb.2007.07.023 [arXiv:0706.4071 [hep-ph]].

- [5] T. Abe, M. Fujiwara, J. Hisano and K. Matsushita, *JHEP* **07** (2020), 136 [arXiv:2004.00884 [hep-ph]].
- [6] T. Abe, M. Fujiwara, J. Hisano and K. Matsushita, *JHEP* **10**, 163 (2021) doi:10.1007/JHEP10(2021)163 [arXiv:2107.10029 [hep-ph]].
- [7] C. Grojean and G. Servant, *Phys. Rev. D* **75** (2007), 043507 doi:10.1103/PhysRevD.75.043507 [arXiv:hep-ph/0607107 [hep-ph]].
- [8] H. Audley *et al.*, “Laser Interferometer Space Antenna,” [arXiv:1702.00786 [astro-ph.IM]].
- [9] N. Seto, S. Kawamura and T. Nakamura, *Phys. Rev. Lett.* **87**, 221103 (2001) [arXiv:astro-ph/0108011 [astro-ph]].
- [10] S. Phinney *et al.*, The Big Bang Observer: Direct detection of gravitational waves from the birth of the Universe to the Present, NASA Mission Concept Study (2004).
- [11] P. Schwaller, *Phys. Rev. Lett.* **115** (2015) no.18, 181101 doi:10.1103/PhysRevLett.115.181101 [arXiv:1504.07263 [hep-ph]].
- [12] M. Chala, G. Nardini and I. Sobolev, *Phys. Rev. D* **94** (2016) no.5, 055006 doi:10.1103/PhysRevD.94.055006 [arXiv:1605.08663 [hep-ph]].
- [13] I. Baldes, *JCAP* **05** (2017), 028 doi:10.1088/1475-7516/2017/05/028 [arXiv:1702.02117 [hep-ph]].
- [14] W. Chao, H. K. Guo and J. Shu, *JCAP* **09** (2017), 009 doi:10.1088/1475-7516/2017/09/009 [arXiv:1702.02698 [hep-ph]].
- [15] A. Beniwal, M. Lewicki, J. D. Wells, M. White and A. G. Williams, *JHEP* **08** (2017), 108 doi:10.1007/JHEP08(2017)108 [arXiv:1702.06124 [hep-ph]].
- [16] A. Addazi and A. Marciano, *Chin. Phys. C* **42** (2018) no.2, 023107 doi:10.1088/1674-1137/42/2/023107 [arXiv:1703.03248 [hep-ph]].
- [17] K. Tsumura, M. Yamada and Y. Yamaguchi, *JCAP* **07** (2017), 044 doi:10.1088/1475-7516/2017/07/044 [arXiv:1704.00219 [hep-ph]].
- [18] F. P. Huang and J. H. Yu, *Phys. Rev. D* **98** (2018) no.9, 095022 doi:10.1103/PhysRevD.98.095022 [arXiv:1704.04201 [hep-ph]].
- [19] F. P. Huang and C. S. Li, *Phys. Rev. D* **96** (2017) no.9, 095028 doi:10.1103/PhysRevD.96.095028 [arXiv:1709.09691 [hep-ph]].
- [20] A. Hektor, K. Kannike and V. Vaskonen, *Phys. Rev. D* **98** (2018) no.1, 015032 doi:10.1103/PhysRevD.98.015032 [arXiv:1801.06184 [hep-ph]].
- [21] K. Hashino, M. Kakizaki, S. Kanemura, P. Ko and T. Matsui, *JHEP* **06** (2018), 088 doi:10.1007/JHEP06(2018)088 [arXiv:1802.02947 [hep-ph]].
- [22] I. Baldes and C. Garcia-Cely, *JHEP* **05** (2019), 190 doi:10.1007/JHEP05(2019)190 [arXiv:1809.01198 [hep-ph]].
- [23] E. Madge and P. Schwaller, *JHEP* **02** (2019), 048 doi:10.1007/JHEP02(2019)048 [arXiv:1809.09110 [hep-ph]].
- [24] A. Beniwal, M. Lewicki, M. White and A. G. Williams, *JHEP* **02** (2019), 183 doi:10.1007/JHEP02(2019)183 [arXiv:1810.02380 [hep-ph]].
- [25] L. Bian and Y. L. Tang, *JHEP* **12** (2018), 006 [arXiv:1810.03172 [hep-ph]].

- [26] Y. Bai, A. J. Long and S. Lu, Phys. Rev. D **99** (2019) no.5, 055047
doi:10.1103/PhysRevD.99.055047 [arXiv:1810.04360 [hep-ph]].
- [27] L. Bian and X. Liu, Phys. Rev. D **99** (2019) no.5, 055003 doi:10.1103/PhysRevD.99.055003
[arXiv:1811.03279 [hep-ph]].
- [28] V. R. Shajjee and A. Tofighi, Eur. Phys. J. C **79** (2019) no.4, 360
doi:10.1140/epjc/s10052-019-6881-6 [arXiv:1811.09807 [hep-ph]].
- [29] A. Mohamadnejad, Eur. Phys. J. C **80** (2020) no.3, 197 doi:10.1140/epjc/s10052-020-7756-6
[arXiv:1907.08899 [hep-ph]].
- [30] G. Bertone, D. Croon, M. A. Amin, K. K. Boddy, B. J. Kavanagh, K. J. Mack, P. Natarajan,
T. Opferkuch, K. Schutz and V. Takhistov, *et al.* SciPost Phys. Core **3** (2020), 007
doi:10.21468/SciPostPhysCore.3.2.007 [arXiv:1907.10610 [astro-ph.CO]].
- [31] K. Kannike, K. Loos and M. Raidal, Phys. Rev. D **101** (2020) no.3, 035001
doi:10.1103/PhysRevD.101.035001 [arXiv:1907.13136 [hep-ph]].
- [32] A. Paul, B. Banerjee and D. Majumdar, JCAP **10** (2019), 062
doi:10.1088/1475-7516/2019/10/062 [arXiv:1908.00829 [hep-ph]].
- [33] E. Hall, T. Konstandin, R. McGehee, H. Murayama and G. Servant, JHEP **04** (2020), 042
[arXiv:1910.08068 [hep-ph]].
- [34] D. Croon, A. Kusenko, A. Mazumdar and G. White, Phys. Rev. D **101** (2020) no.8, 085010
doi:10.1103/PhysRevD.101.085010 [arXiv:1910.09562 [hep-ph]].
- [35] N. Chen, T. Li, Y. Wu and L. Bian, Phys. Rev. D **101** (2020) no.7, 075047
doi:10.1103/PhysRevD.101.075047 [arXiv:1911.05579 [hep-ph]].
- [36] E. Hall, T. Konstandin, R. McGehee and H. Murayama, [arXiv:1911.12342 [hep-ph]].
- [37] B. Barman, A. Dutta Banik and A. Paul, Phys. Rev. D **101** (2020) no.5, 055028
doi:10.1103/PhysRevD.101.055028 [arXiv:1912.12899 [hep-ph]].
- [38] C. W. Chiang and B. Q. Lu, JHEP **07** (2020), 082 doi:10.1007/JHEP07(2020)082
[arXiv:1912.12634 [hep-ph]].
- [39] D. Borah, A. Dasgupta, K. Fujikura, S. K. Kang and D. Mahanta, JCAP **08** (2020), 046
doi:10.1088/1475-7516/2020/08/046 [arXiv:2003.02276 [hep-ph]].
- [40] Z. Kang and J. Zhu, Phys. Rev. D **102** (2020) no.5, 053011
doi:10.1103/PhysRevD.102.053011 [arXiv:2003.02465 [hep-ph]].
- [41] M. Pandey and A. Paul, [arXiv:2003.08828 [hep-ph]].
- [42] J. P. Hong, S. Jung and K. P. Xie, Phys. Rev. D **102** (2020) no.7, 075028
doi:10.1103/PhysRevD.102.075028 [arXiv:2008.04430 [hep-ph]].
- [43] T. Alanne, N. Benincasa, M. Heikinheimo, K. Kannike, V. Keus, N. Koivunen and
K. Tuominen, JHEP **10** (2020), 080 doi:10.1007/JHEP10(2020)080 [arXiv:2008.09605
[hep-ph]].
- [44] A. Bhoonah, J. Bramante, S. Nerval and N. Song, JCAP **04** (2021), 043
doi:10.1088/1475-7516/2021/04/043 [arXiv:2008.12306 [hep-ph]].
- [45] X. F. Han, L. Wang and Y. Zhang, Phys. Rev. D **103** (2021) no.3, 035012
doi:10.1103/PhysRevD.103.035012 [arXiv:2010.03730 [hep-ph]].

- [46] Y. Wang, C. S. Li and F. P. Huang, Phys. Rev. D **104** (2021) no.5, 053004 doi:10.1103/PhysRevD.104.053004 [arXiv:2012.03920 [hep-ph]].
- [47] T. Ghosh, H. K. Guo, T. Han and H. Liu, JHEP **07** (2021), 045 doi:10.1007/JHEP07(2021)045 [arXiv:2012.09758 [hep-ph]].
- [48] W. C. Huang, M. Reichert, F. Sannino and Z. W. Wang, Phys. Rev. D **104** (2021) no.3, 035005 doi:10.1103/PhysRevD.104.035005 [arXiv:2012.11614 [hep-ph]].
- [49] X. Deng, X. Liu, J. Yang, R. Zhou and L. Bian, Phys. Rev. D **103** (2021) no.5, 055013 doi:10.1103/PhysRevD.103.055013 [arXiv:2012.15174 [hep-ph]].
- [50] W. Chao, X. F. Li and L. Wang, JCAP **06** (2021), 038 doi:10.1088/1475-7516/2021/06/038 [arXiv:2012.15113 [hep-ph]].
- [51] A. Azatov, M. Vanvlasselaer and W. Yin, JHEP **03** (2021), 288 doi:10.1007/JHEP03(2021)288 [arXiv:2101.05721 [hep-ph]].
- [52] Z. Zhang, C. Cai, X. M. Jiang, Y. L. Tang, Z. H. Yu and H. H. Zhang, JHEP **05** (2021), 160 doi:10.1007/JHEP05(2021)160 [arXiv:2102.01588 [hep-ph]].
- [53] H. Davoudiasl, P. B. Denton and J. Gehrlein, Phys. Rev. Lett. **128** (2022) no.8, 081101 doi:10.1103/PhysRevLett.128.081101 [arXiv:2109.01678 [astro-ph.CO]].
- [54] M. Reichert, F. Sannino, Z. W. Wang and C. Zhang, JHEP **01** (2022), 003 doi:10.1007/JHEP01(2022)003 [arXiv:2109.11552 [hep-ph]].
- [55] A. Mohamadnejad, JHEP **03** (2022), 188 doi:10.1007/JHEP03(2022)188 [arXiv:2111.04342 [hep-ph]].
- [56] L. Bian, Y. L. Tang and R. Zhou, Phys. Rev. D **106** (2022) no.3, 035028 doi:10.1103/PhysRevD.106.035028 [arXiv:2111.10608 [hep-ph]].
- [57] F. Costa, S. Khan and J. Kim, JHEP **06** (2022), 026 doi:10.1007/JHEP06(2022)026 [arXiv:2202.13126 [hep-ph]].
- [58] X. Liu, S. Y. Guo, B. Zhu and Y. Li, Sci. Bull. **67** (2022), 1437-1442 doi:10.1016/j.scib.2022.06.011 [arXiv:2204.04834 [hep-ph]].
- [59] H. Shibuya and T. Toma, JHEP **11** (2022), 064 doi:10.1007/JHEP11(2022)064 [arXiv:2207.14662 [hep-ph]].
- [60] F. Costa, S. Khan and J. Kim, JHEP **12** (2022), 165 doi:10.1007/JHEP12(2022)165 [arXiv:2209.13653 [hep-ph]].
- [61] M. Kierkla, A. Karam and B. Swiezewska, [arXiv:2210.07075 [astro-ph.CO]].
- [62] E. Morgante, N. Ramberg and P. Schwaller, Phys. Rev. D **107** (2023) no.3, 3 doi:10.1103/PhysRevD.107.036010 [arXiv:2210.11821 [hep-ph]].
- [63] N. Chakrabarty, H. Roy and T. Srivastava, [arXiv:2212.09659 [hep-ph]].
- [64] G. Arcadi, N. Benincasa, A. Djouadi and K. Kannike, [arXiv:2212.14788 [hep-ph]].
- [65] M. T. Frandsen, M. E. Thing, M. Heikinheimo, K. Tuominen and M. Rosenlyst, [arXiv:2301.00041 [hep-ph]].
- [66] G. Aad *et al.* [ATLAS], Phys. Rev. D **101** (2020) no.1, 012002 doi:10.1103/PhysRevD.101.012002 [arXiv:1909.02845 [hep-ex]].

- [67] [ATLAS], Nature **607** (2022) no.7917, 52-59 [erratum: Nature **612** (2022) no.7941, E24] doi:10.1038/s41586-022-04893-w [arXiv:2207.00092 [hep-ex]].
- [68] E. Aprile *et al.* [XENON], JCAP **04** (2016), 027 doi:10.1088/1475-7516/2016/04/027 [arXiv:1512.07501 [physics.ins-det]].
- [69] C. Grojean, G. Servant and J. D. Wells, Phys. Rev. D **71** (2005), 036001 doi:10.1103/PhysRevD.71.036001 [arXiv:hep-ph/0407019 [hep-ph]].
- [70] K. Hashino and D. Ueda, [arXiv:2210.11241 [hep-ph]].
- [71] G. W. Anderson and L. J. Hall, Phys. Rev. D **45** (1992), 2685-2698
- [72] C. Delaunay, C. Grojean and J. D. Wells, JHEP **04** (2008), 029 [arXiv:0711.2511 [hep-ph]].
- [73] T. Hahn, Comput. Phys. Commun. **140** (2001), 418-431 doi:10.1016/S0010-4655(01)00290-9 [arXiv:hep-ph/0012260 [hep-ph]].
- [74] T. Hahn and M. Perez-Victoria, Comput. Phys. Commun. **118** (1999), 153-165 doi:10.1016/S0010-4655(98)00173-8 [arXiv:hep-ph/9807565 [hep-ph]].
- [75] L. Dolan and R. Jackiw, Phys. Rev. D **9**, 3320 (1974).
- [76] R. R. Parwani, Phys. Rev. D **45** (1992), 4695 [erratum: Phys. Rev. D **48** (1993), 5965] [arXiv:hep-ph/9204216 [hep-ph]].
- [77] P. B. Arnold and O. Espinosa, Phys. Rev. D **47** (1993), 3546 [erratum: Phys. Rev. D **50** (1994), 6662] [arXiv:hep-ph/9212235 [hep-ph]].
- [78] A. D. Linde, Nucl. Phys. B **216** (1983), 421 [erratum: Nucl. Phys. B **223** (1983), 544]
- [79] S. R. Coleman, Phys. Rev. D **15** (1977), 2929-2936 [erratum: Phys. Rev. D **16** (1977), 1248]
- [80] L. Li, S. J. Wang and Z. Y. Yuwen, [arXiv:2302.10042 [hep-th]].
- [81] D. Bodeker and G. D. Moore, JCAP **05** (2009), 009 [arXiv:0903.4099 [hep-ph]].
- [82] D. Bodeker and G. D. Moore, JCAP **05** (2017), 025 [arXiv:1703.08215 [hep-ph]].
- [83] A. Kosowsky, A. Mack and T. Kahniashvili, Phys. Rev. D **66** (2002), 024030 [arXiv:astro-ph/0111483 [astro-ph]].
- [84] M. Hindmarsh, S. J. Huber, K. Rummukainen and D. J. Weir, Phys. Rev. D **92** (2015) no.12, 123009 [arXiv:1504.03291 [astro-ph.CO]].
- [85] C. Caprini, M. Chala, G. C. Dorsch, M. Hindmarsh, S. J. Huber, T. Konstandin, J. Kozaczuk, G. Nardini, J. M. No and K. Rummukainen, *et al.* JCAP **03** (2020), 024 [arXiv:1910.13125 [astro-ph.CO]].
- [86] M. Hindmarsh, S. J. Huber, K. Rummukainen and D. J. Weir, Phys. Rev. D **96** (2017) no.10, 103520 [erratum: Phys. Rev. D **101** (2020) no.8, 089902] [arXiv:1704.05871 [astro-ph.CO]].
- [87] J. R. Espinosa, T. Konstandin, J. M. No and G. Servant, JCAP **06** (2010), 028 doi:10.1088/1475-7516/2010/06/028 [arXiv:1004.4187 [hep-ph]].
- [88] N. Seto, Phys. Rev. D **73** (2006), 063001 [arXiv:gr-qc/0510067 [gr-qc]].
- [89] K. Yagi and N. Seto, Phys. Rev. D **83** (2011), 044011 [erratum: Phys. Rev. D **95** (2017) no.10, 109901] [arXiv:1101.3940 [astro-ph.CO]].
- [90] A. Klein, E. Barausse, A. Sesana, A. Petiteau, E. Berti, S. Babak, J. Gair, S. Aoudia, I. Hinder and F. Ohme, *et al.* Phys. Rev. D **93** (2016) no.2, 024003 [arXiv:1511.05581 [gr-qc]].

- [91] C. Caprini, M. Hindmarsh, S. Huber, T. Konstandin, J. Kozaczuk, G. Nardini, J. M. No, A. Petiteau, P. Schwaller and G. Servant, *et al.* JCAP **04** (2016), 001 [arXiv:1512.06239 [astro-ph.CO]].
- [92] A. Eichhorn, J. Lumma, J. M. Pawlowski, M. Reichert and M. Yamada, JCAP **05** (2021), 006 [arXiv:2010.00017 [hep-ph]].